2007-07-09

Extreme Ultraviolet Polarimetry with Laser-Generated High-Order Harmonics

Nicole Brimhall
Brigham Young University - Provo

EXTREME ULTRAVIOLET POLARIMETRY WITH LASER-GENERATED HIGH-ORDER HARMONICS

by

Nicole Brimhall

A thesis submitted to the faculty of

Brigham Young University

in partial fulfillment of the requirements for the degree of

Master of Science

Department of Physics and Astronomy

Brigham Young University

August 2007

BRIGHAM YOUNG UNIVERSITY

GRADUATE COMMITTEE APPROVAL

of a thesis submitted by

Nicole Brimhall

This thesis has been read by each member of the following graduate committee and by majority vote has been found to be satisfactory.

Date	Justin B. Peatross, Chair
Date	R. Steven Turley
Date	David D. Allred

BRIGHAM YOUNG UNIVERSITY

As chair of the candidate's graduate committee, I have read the thesis of Nicole Brimhall in its final form and have found that (1) its format, citations, and bibliographical style are consistent and acceptable and fulfill university and department style requirements; (2) its illustrative materials including figures, tables, and charts are in place; and (3) the final manuscript is satisfactory to the graduate committee and is ready for submission to the university library.

Date

Justin B. Peatross
Chair, Graduate Committee

Accepted for the Department

Ross L. Spencer, Department Chair
Department of Physics and Astronomy

Accepted for the College

Thomas W. Sederberg, Associate Dean
College of Physical and Mathematical Sciences

ABSTRACT

EXTREME ULTRAVIOLET POLARIMETRY WITH LASER-GENERATED HIGH-ORDER HARMONICS

Nicole Brimhall

Department of Physics and Astronomy

Master of Science

We developed an extreme ultraviolet (EUV) polarimeter, which employs laser-generated high-order harmonics as the light source. This relatively high-flux directional EUV source has available wavelengths between 8 nm and 62 nm and easily rotatable linear polarization. The polarimeter will aid researchers at BYU in characterizing EUV thin films and improving their understanding of materials for use in EUV optics. This first-time workhorse application of laser high harmonics enables polarization-sensitive reflection measurements not previously available in the EUV. We have constructed a versatile positioning system that places harmonics on the microchannel plate detector with an accuracy of 0.3 mm, which allows a spectral resolution of about 180. We have demonstrated that reflectance as low as 0.2% can be measured at EUV wavelengths and that this data is repeatable to within the error of our source stability (∼7% fluctuation). We have compared reflectance data with that

taken from the same sample at Beamline 6.3.2 at the Advanced Light Source. This data agrees well from 5 degrees to 30 degrees and the angular locations of the interference fringes also agree.

ACKNOWLEDGMENTS

I would like to acknowledge my advisor, Justin Peatross for all of his support and assistance. Also, thank you to all of the students and advisors of the EUV research group and the students of the high harmonics research group at BYU for their contribution to this work. I would especially like to recognize my husband Bryan and my family for their patient encouragement of my goals. I would also like to thank the National Science Foundation for supporting this research (Grant# PHY-0457316).

Contents

List of Figures

Chapter 1

Introduction

1.1 The Extreme Ultraviolet: Background and Applications

The extreme ultraviolet (EUV), the region in the electromagnetic spectrum from 1 nm to 100 nm, is becoming increasingly important in fields such as lithography for producing integrated circuits, space-based astronomy, and microscopy. However, there are many difficulties in working in this wavelength region. In particular, nearly all materials are highly absorbing in the EUV. This virtually precludes the use of transmissive optics and necessitates multilayer reflective optics. Materials used for such optics need to be highly reflecting, and their indices of refraction should be well known. However, in this region, there are not many materials that provide for high reflectance, and the optical properties of the majority of materials are unknown or incomplete. This incomplete information poses a problem for designing optics for varied applications.

The EUV research group at Brigham Young University (BYU), directed by Professor David Allred and Professor Steve Turley, produced mirror coatings that were

used on the IMAGE satellite, which was launched March 25, 2000 [1]. This instrument took the first series of pictures of the Earth's magnetosphere at 41 eV as part of a comprehensive multi-spectral imaging of the near-space around Earth. The mirror coatings used in the satellite needed high reflectance (greater than 20%) at 30.4 nm, 14 degrees from normal and low reflectance (less than 2%) at 58.4 nm. The design work for this project was hampered by the fact that the index of refraction, or optical constants, for several of the coating materials differed significantly from published values, forcing remeasurement of the values themselves. Researchers in the last decade, including those at BYU, have realized the need to expand and verify optical constants of materials in the EUV.

The complex index of refraction of a material is obtained by measuring reflectance and/or transmittance of the material as a function of sample angle, wavelength, and polarization. Reflectance or transmittance measurements are defined as reflected or transmitted light intensity divided by incident light intensity, giving a percentage reflected or transmitted light for each sample angle.

Reflectance or transmittance data is fit to the Fresnel coefficients to obtain the complex index of refraction, N, which includes the real part, n, and the imaginary part, κ. n and κ are essentially interchangeable with the commonly used δ and β, where $n = 1 - \delta$ and $\kappa = \beta$. The set of n and κ (or δ and β) are referred to as optical constants. Currently in the EUV research group at BYU, reflectance and transmittance measurements are made either at BYU using a monochromator with a plasma light source or at the Advanced Light Source (ALS) synchrotron at Lawrence Berkeley National Labs in Berkeley, California. The process of making reflectance measurements is commonly referred to as reflectometry. When reflectometry is performed using a polarized light source, the process is called polarimetry.

Previous work in the EUV group includes measuring the optical constants of

uranium, uranium oxides [2], uranium nitride [3], thorium [4], thorium dioxide [5], and scandium oxide [6]. Figure 1.1 depicts the optical constants of thorium dioxide measured by the EUV research group at BYU compared with those determined previously by other groups [5, 7]. The discrepancies seen in this plot emphasize the need for accurate remeasurement of many sets of published optical constants.

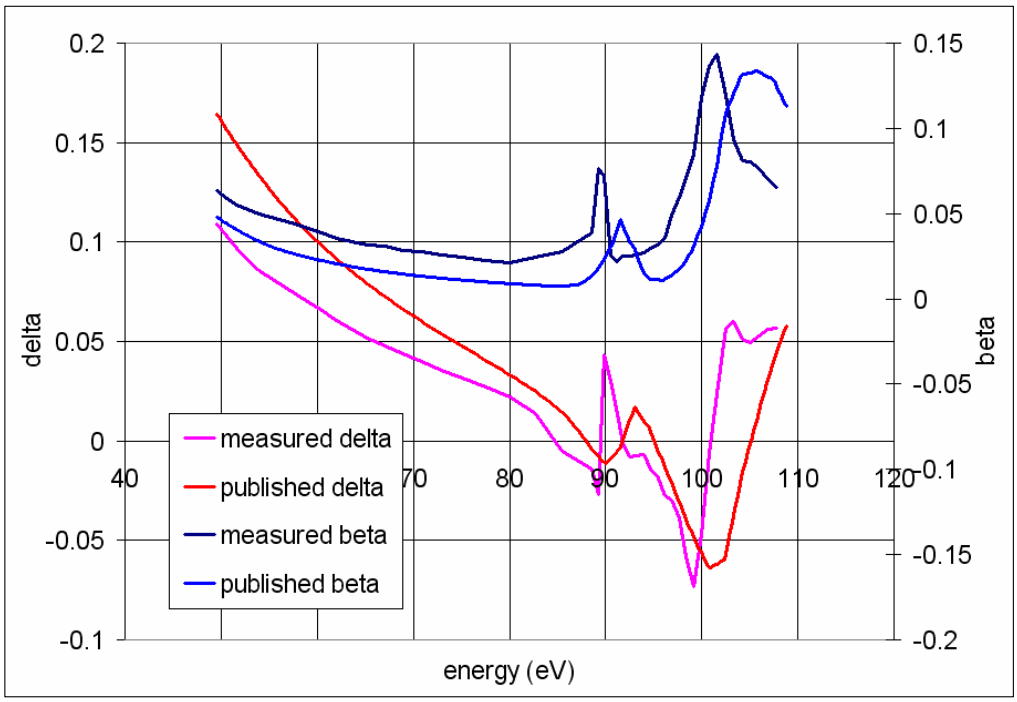

Figure 1.1 Graph of published optical constants of thorium dioxide [7] versus values measured by the BYU EUV research group [5].

Along these same lines, the EUV research group at BYU has also furthered techniques for determining optical constants to a greater degree of accuracy. These techniques include measuring and fitting reflectance and transmittance data simultaneously [8], determining the effect of surface roughness and interfacial diffusion on reflectance data [9], and determining the accuracy of utilizing Kramers-Kronig relations to find optical constants [10]. All of these important developments in the understanding of materials in the EUV are hampered by the fact that BYU's monochromator

does not have the flux nor the wavelength range of the ALS. However, the ALS is located in Berkeley, California, requiring significant time and travel expenses to make measurements there. Because optical properties are intertwined with surface characteristics and thin-film preparation procedures, it will be a big advantage to have a polarimeter with sufficient source brightness and energy range co-located with sample preparation and characterization instruments at BYU.

1.2 High Harmonic Generation

Laser-generated high harmonics provide an excellent source of polarized, directional EUV light. This thesis outlines the development of EUV polarimetry using available high harmonics at BYU. The harmonics form a comb of frequencies throughout the EUV, in our case ranging from 8 nm to 62 nm. The wavelength of an individual harmonic is λ/q, where λ is the wavelength of the generating laser and q is the harmonic order, an odd integer. The odd harmonics of 800 nm laser light in principle can be generated up to several hundred orders [11–13]. Harmonics are generated when a short-pulsed laser is focused to create high intensities (approximately 10^{15} W/cm^2) in a gas such as argon, neon, or helium. The laser pulses cause strong nonlinear responses in the individual atoms of the gas, generating harmonics that are coherent with the incident beam. Many harmonic frequencies (with wavelengths distributed throughout the EUV) simultaneously emerge from the focus in a collimated beam, which is embedded in the residual laser beam as shown in Figure 1.2. The harmonics include wavelengths in the neighborhood of 13.5 nm (the 59th harmonic), which is the wavelength being developed by the computer chip industry for EUV lithography. The harmonics take on the same linear polarization as the incident laser light [14].

Our high harmonics are generated with 800 nm, 30 fs, ∼10 mJ laser pulses focused

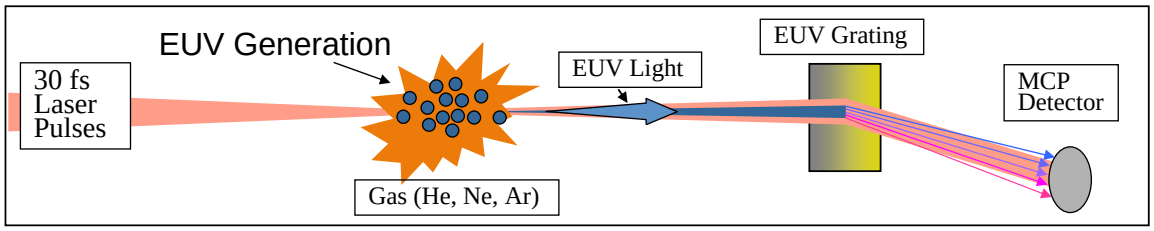

Figure 1.2 Setup for producing high-order harmonics.

in a cell of helium, neon, or argon gas. High harmonics are detected using a grazing-incidence tungsten-coated grating, which disperses and focuses the different harmonic orders onto a microchannel plate (MCP) coupled to a phosphor screen. This setup was used to produce the high harmonics seen in Figure 1.3. Each harmonic order strikes the detector at a different horizontal position while the angular size of each harmonic beam is preserved in the vertical dimension.

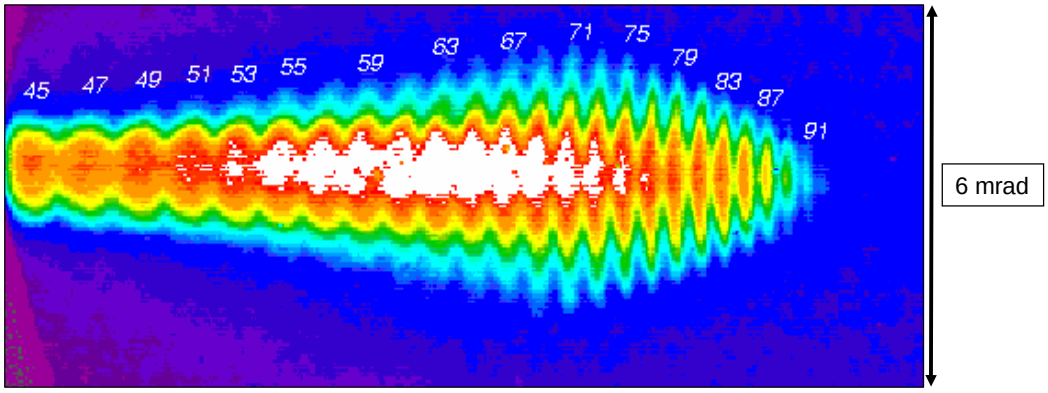

Figure 1.3 Harmonics of order 45-91 (wavelengths 8.8-17.8 nm) produced in neon gas.

High harmonics continue to be a topic of active research. A summary of the characteristics of the harmonics available at BYU are presented in Table 1.1. For comparison, the characteristics of Beamline 6.3.2 at the Advanced Light Source [15] in Berkeley, California, a beamline commonly used for EUV optics testing, and char-

acteristics for the hollow cathode plasma source at BYU are also shown.

As seen in Table 1.1, the wavelength range of high-harmonic EUV is wide, and although it is not continuous like the ALS, it has good spacing of wavelengths throughout the range. Also, many of the higher harmonics merge together, giving it continuous wavelength coverage in some ranges. In contrast, ionic and atomic emission lines from a plasma source are clustered around only a few wavelengths. The flux of high harmonics is relatively high, a factor of 300,000 brighter than BYU's plasma source. On the other hand, the high harmonics are only a factor of 30 dimmer than the ALS, not a huge number when considering the size and cost of operation. The synchrotron is a hundred-million-dollar instrument with a footprint the size of a football field and a permanent staff of hundreds of people [16]. The spectral resolution of high harmonics produced at BYU is not as good as that of the synchrotron or the plasma source, but it is good enough to resolve broad features in optical constant data. The spectral resolution will be discussed further in section 3.4.

One of the great advantages of high harmonics is that the EUV light preserves the same linear polarization as the generating laser beam. Polarized EUV light is difficult to produce using other approaches because EUV light is easily absorbed, and so transmissive polarizers cannot be used with practical efficiency. Multilayer reflective polarizers have been developed, but these are not broadband. Synchrotron light is naturally polarized, but this is not easily rotated. In contrast, the polarization of high harmonic EUV light is easily rotated by placing a half-wave plate in the incident laser beam before the EUV light is generated. In this way we can make polarization-sensitive reflectance measurements at multiple polarizations, something never before done on a regular basis in the EUV. This can further constrain data to achieve accurate optical constants.

Previous work on high harmonics at BYU has made it possible to achieve the

	High Harmonic Generation at BYU	**Beamline 6.3.2 at the Advanced Light Source**	**Hollow Cathode Plasma Source at BYU**
Energy	20-155 eV (8-62 nm), quantized as 1.55q eV where q is a positive odd integer (roughly every 3 eV)	50-1300 eV (1-25 nm) continuous	Various atomic and ionic emission lines from 10-177 eV (7-121.6 nm). Comprises approximately 150 lines.
Flux	6×10^8 photons/sec at 100 eV (measured, comprising 10 laser shots)	1.6×10^{10} photons/sec at 100 eV (calculated)	2×10^3 photons/sec at 41 eV (measured)
Spectral Resolution ($E/\Delta E$)	∼180	1100	500
Polarization	Rotatable linear polarization (same as laser)	Fixed 90% S-polarized, 10% P-polarized	Unpolarized
Detectors	Microchannel plate (MCP)	Photodiode, Channeltron, CCD	Channeltron
Spot Size at Sample	1000×1000 μm	10×300 μm	5000×5000 μm

Table 1.1 Characteristics of high harmonic generation as a source of EUV light compared to two commonly used sources, Beamline 6.3.2 at the Advanced Light Source and a hollow cathode plasma source currently in operation at BYU.

brightness needed to make reflectance measurements at EUV wavelengths. In the past decade, the group of Prof. Justin Peatross at BYU has constructed a high intensity laser system to produce high-order harmonics. Former doctoral student, Sergei Voronov, and former master's student, Julia Sutherland, used counter-propagating light to probe the region where high harmonics are produced [17]. Sutherland found that high harmonics produced in a long gas cell are phase matched over a much longer distance than was expected, an effect which is responsible for unusually bright harmonics [18]. Following up on their work, another master's student, John Painter, and myself observed that a double focusing and flat-top spatial profile in the laser-beam was associated with this extended phase matching [19]. This work will be discussed in Chapter 2.

In addition to their other work, Sutherland and Painter also investigated an effect where harmonic orders are significantly brightened by partially obstructing the laser beam with an aperture prior to harmonic generation. We are still investigating why this happens, but the harmonics have been sufficiently optimized to make them a very useful source for polarimetry.

1.3 Previous Work on an EUV Polarimeter

Voronov and former undergraduate student Greg Harris previously constructed a simple prototype instrument at BYU to make polarization-sensitive reflectometry measurements in the EUV [17]. The fixed-angle instrument utilized laser-generated high harmonics as a source of polarized EUV light. Figure 1.4 shows a schematic of their prototype instrument.

The high harmonics for this prototype experiment were produced in argon gas inside the first chamber. A half wave plate in the generating laser beam controlled

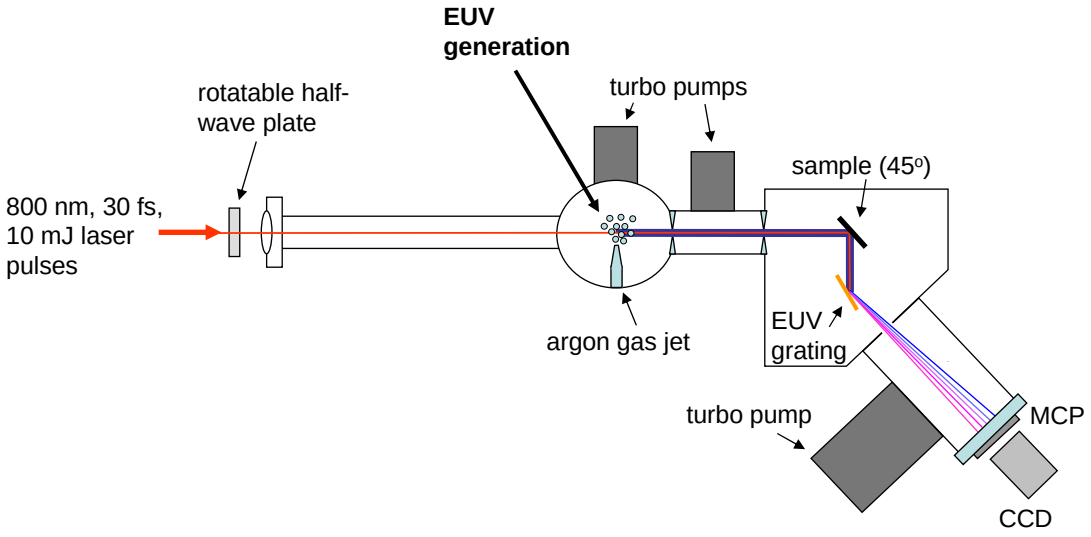

Figure 1.4 Prototype polarimeter (top view). Taken from Voronov [17].

the orientation of the harmonic polarization. Three turbo pumps provided differential pumping to maintain low pressure at the detector. After reflecting off of the sample, the harmonic beams proceeded to a tungsten-coated grating (600 lines/mm, 2° blaze) with a 1 m radius of curvature. They were diffracted and focused by the grating onto an MCP coupled to a phosphor screen.

The prototype experiment included several important features of the full instrument. The polarization of the incident harmonics could be easily rotated with the half wave plate in the laser beam. Also, because the grating was placed after the sample, reflectance of multiple wavelengths of EUV light could be measured simultaneously. This instrument demonstrated that the harmonic source would have sufficient brightness to measure reflectances as low as 0.5% at low to moderate harmonic orders.

The major limitation of this prototype instrument was its lack of scanning mobility. The sample was at a fixed angle of 45°, only one data point in a measurement of reflectance as a function of angle. Also, the sample could not be moved out of the

beam in order to measure incident light intensity. To remedy this, a 'reference' wafer was placed on the sample stage at the same time as the 'sample' wafer, such that the harmonic beams were cut in half as each half reflected from a different surface. Presumably, reflected signal from the 'reference' or known sample could be used to deduce the incident signal. This could then be employed to determine the reflectance from the unknown sample.

In this case, both the 'sample' and 'reference' wafers were silicon substrates with different oxide thicknesses. Figure 1.5 shows the harmonics at the MCP after having reflected from both wafers simultaneously. Figure 1.6 shows a comparison between the s- and p-polarized reflected high-harmonic light from the two surfaces. The two surfaces show significant differences in reflectivity, presumably owing to their different oxide layer thicknesses. This prototype data, although limited, gave us confidence that the full scale instrument would have sufficient brightness to make reflectance measurements at these wavelengths.

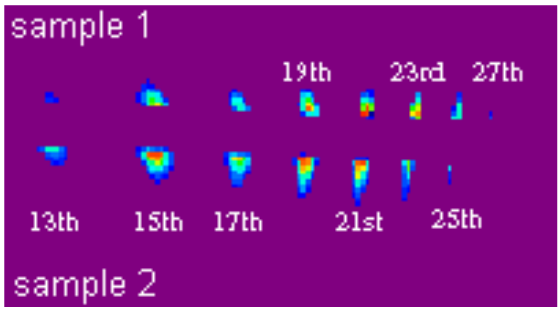

Figure 1.5 Harmonics reflected from two different samples. Taken from Voronov [17].

1.4 Overview of New Instrument and Outcomes

For my thesis, I constructed a full scale polarimeter instrument with extensive scanning capabilities, which allows us to characterize optical surfaces in the EUV on a

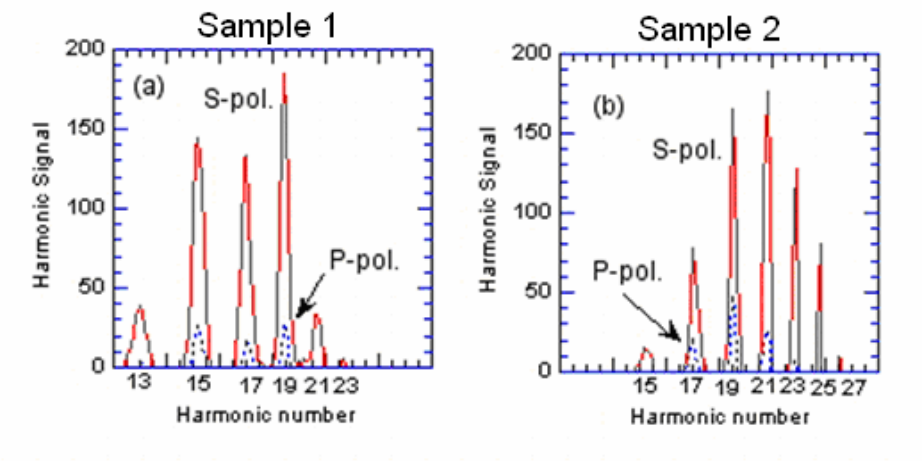

Figure 1.6 S-polarized vs. p-polarized high harmonics reflected from two silicon wafers with different oxide thicknesses. Taken from Voronov [17].

routine basis. To our knowledge, this is the first time that high harmonics have been employed in a workhorse setting, as opposed to merely demonstrating proof of concept. The full instrument can determine the reflectance from samples as a function of incident angle, light polarization orientation, and wavelength (associated with a discrete comb of odd harmonics of 800 nm, up to order ∼99). As with the prototype instrument, we are able to measure reflectance from a wide comb of wavelengths simultaneously (with a much wider range of available wavelengths due to a rotatable grating), and the polarization of the incident light is easily rotated with a half-wave plate in the incident beam. A schematic of the full scale instrument is shown in Figure 1.7.

We have found that our high harmonic source has enough flux to measure reflectances as low as 0.2% with an energy range from 8 nm to 62 nm. By averaging multiple laser shots, we have shown that our incident light intensity is stable to within 7%. Our positioning system is robust and versatile and is able to achieve a

spectral resolution ($\lambda/\Delta\lambda$) of about 180. We have measured reflectance as a function of angle of a thermally oxidized silicon sample and found that these measurements were repeatable to within our source stability. We have also compared these measurements with measurements taken at Beamline 6.3.2 of the Advanced Light Source in Berkeley, California. The two measurements agreed very well from 5 degrees to 30 degrees. Above 30 degrees the polarimeter measurements read about a factor of four too high, but were qualitatively consistent with ALS data. This may be caused by an incorrectly calibrated microchannel plate, which can be corrected in the future.

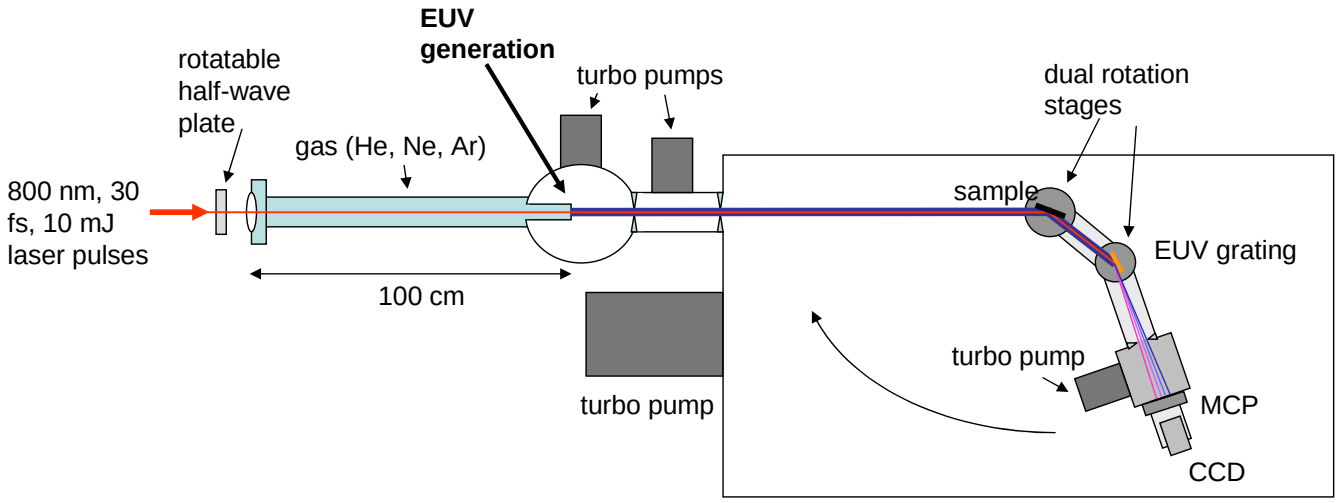

Figure 1.7 The full scale polarimeter.

Chapter 2

High Harmonic Source

In this chapter we discuss the high harmonic source itself. We characterized the spatial evolution of the laser pulse energy distribution as it propagated within a gas cell [20, 21]. We also documented the evolution of the brightness of the associated high-harmonic emission. These measurements show evidence of self guiding and even refocusing of the laser energy, which would seem suggestive of Kerr-style filamentation. However, the laser power used in the experiment is well below the critical power for filamentation [22–24]. An alternative explanation has since been developed by Matthew Turner, another member of our research group.

2.1 High Harmonic Generation

The laser system we use to generate harmonics is a Ti:sapphire, 10 mJ laser that delivers pulses at a repetition rate of 10 Hz. The laser pulses are centered on 800 nm with a bandwidth of 35 nm (FWHM). The pulse duration measured by autocorrelation was determined to be 30 fs. The laser beam is focused with a 100 cm focal length lens or mirror into a cell filled with helium, neon, or argon gas (see Figure 2.1).

This focusing achieved an intensity of 1.9×10^{15} W/cm^2 (with 25% uncertainty) in vacuum and approximately half that in the gas-filled cell which modified the focus. An 8-10 mm aperture (closed on a ∼2 cm beam) located before the focusing optic was shown to strongly enhance harmonic emission [25]. A glass tube capped with molybdenum foil separates the region of gas from vacuum. This setup, where the gas filled region extends from the focusing optic to the molybdenum foil, is called a semi-infinite gas cell configuration and was shown to produce brighter harmonics than short cells of 6 mm or less [18]. The laser self drills a hole in the molybdenum foil, eliminating the need for precise alignment. After harmonic generation, the harmonics exit into vacuum and co-propagate with the residual laser beam. The harmonics and laser proceed to the detection setup about 1.5 m away, passing through two pinholes that provide for differential pumping. The harmonics are separated and focused in one dimension by a tungsten-coated EUV grating and are detected by a microchannel plate detector coupled to a phosphor screen. A visible light CCD camera captures the image on the phosphor screen and relays it to the computer.

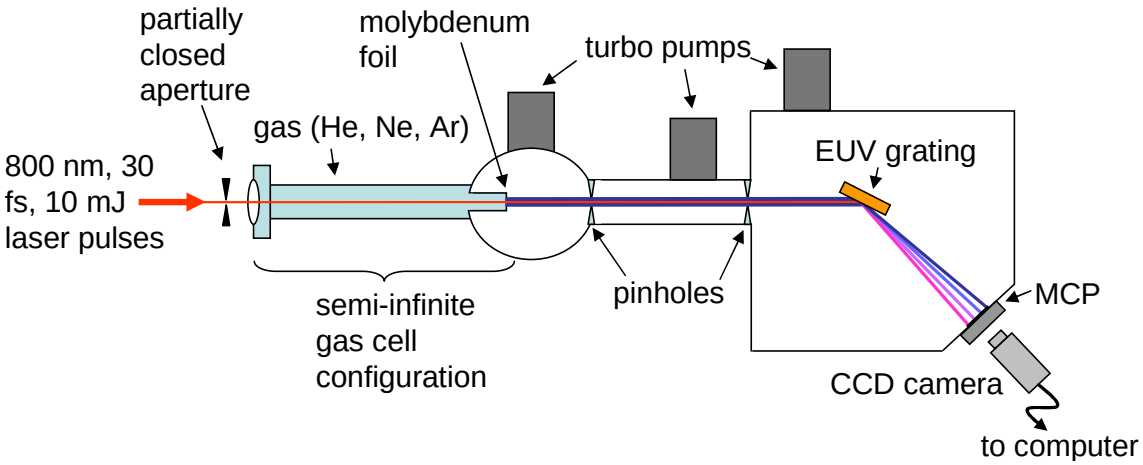

Figure 2.1 Harmonic generation and detection setup.

Figure 2.2 shows harmonics produced in 80 torr helium from the 45th to the 91st

order, which have approximately uniform intensity. We measured the energy in an individual harmonic order to be approximately 1 nJ [21]. Higher order harmonics are diffracted with a 1200 line/mm grating with 2 m radius of curvature while lower order harmonics are diffracted with a 600 line/mm grating with a 1 m radius of curvature. We found that the best gas pressure for harmonic production in helium is about 80 torr and the best gas pressure for harmonic production in neon is about 50 torr. The intensity of the harmonics is not affected by gas pressure variation of ±4 torr.

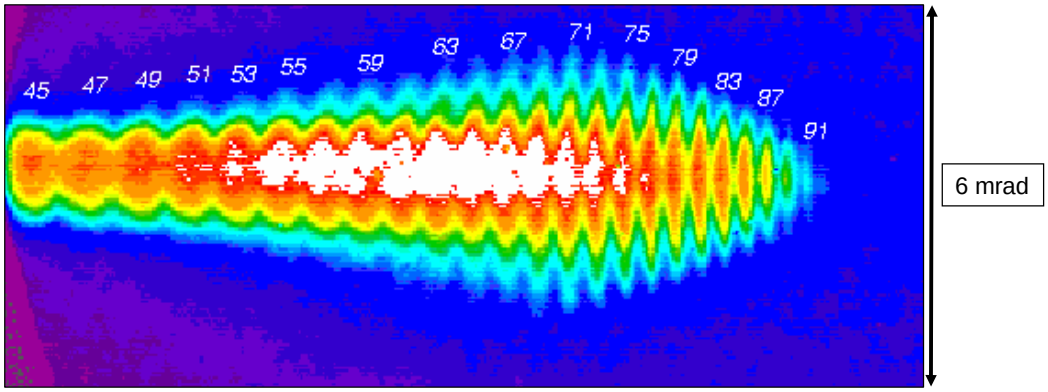

Figure 2.2 Harmonics of order 45-91 (wavelengths 8.8-17.8 nm) produced in neon gas.

2.2 Previous Work

Previously, Sutherland, *et al.* [26] used counter-propagating pulses to probe the region near the focus where harmonics are generated. They observed that in neon the harmonics are generated in the last few millimeters before the exit foil, and in helium the harmonics are produced over many millimeters. Former undergraduate Eric Christensen [27] found that the difference in the harmonic generation depths as characterized by the counter-propagating light is consistent with the differences in absorption rates of the two gases. Christensen measured gas absorption by placing a

second gas cell after harmonic production and measuring harmonic signal attenuation as gas pressure in the second cell was increased. Transmission of the 71st harmonic through 2 mm of 55 torr neon was found to be 29%; in contrast, the 71st harmonic was found to propagate through 10 mm in helium at 115 torr with the same level of absorption.

The above measurements suggest that harmonics are phase matched over many millimeters, limited primarily by absorption. This is unexpectedly long, since the natural diffraction of a free laser beam should introduce phase mismatches that limit the coherence lengths to a fraction of a millimeter. This extended phase matching suggests that laser self guiding plays a role in enhancing harmonic production in gas cells, a proposition supported by reports made by Tamaki, *et al.* [28] based on the observation of strong harmonic emission from thick gas cells. Former master's student, John Painter, and myself investigated the possibility that laser filamentation was causing this extended phase matching [19]. We did this by characterizing the spatial profile of the generating laser beam in the region of harmonic production.

2.3 Effect of Focal Position on Harmonic Generation and Laser Profile

To image the spatial profile of the laser beam under conditions suitable for producing harmonics, an uncoated glass substrate oriented at 45 degrees was temporarily inserted in the beam before the harmonic-detection setup (see Figure 2.3). The glass substrate, which functioned both as a mirror and an attenuator, could be moved into and out of the laser beam in a matter of seconds while maintaining vacuum in the harmonic detection setup. The substrate reflected approximately 2% of the laser, which was imaged by an f = 75 cm focusing lens onto a CCD camera. Neutral density filters

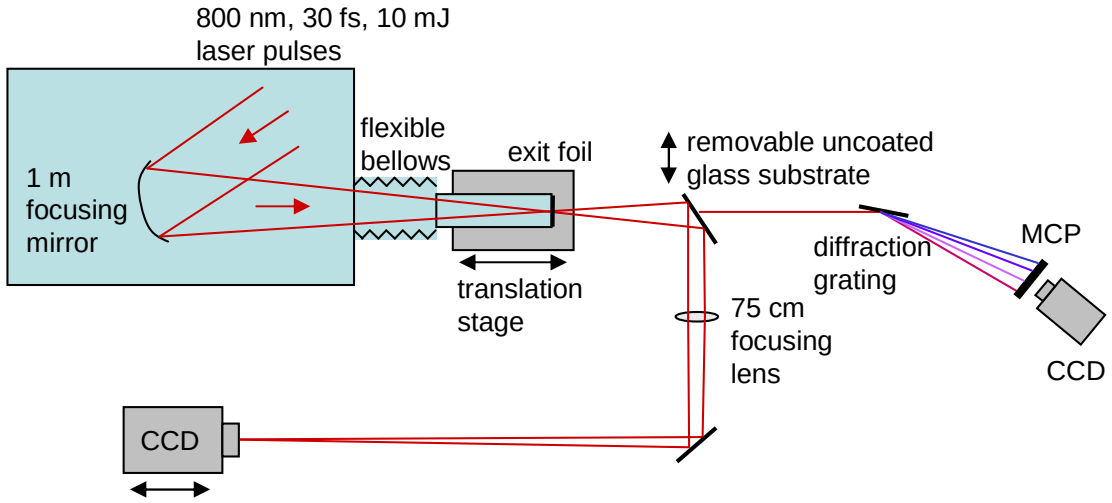

Figure 2.3 Setup to image laser beam spatial profile under conditions suitable for harmonic generation.

were used for further attenuation. The camera was positioned to image the laser at the plane of the exit foil of the gas cell. The position of the foil was scanned parallel to the laser axis over a range of 9 cm. The axial position of the camera was also scanned to maintain an image of the laser beam at the exit foil. The magnification of the image was approximately 3×, depending on the exact location of the foil relative to the imaging lens.

Figure 2.4 shows harmonics generated in 80 torr helium gas together with the laser beam spatial profile at the z = 0 cm position, or where the beam focuses in vacuum. The left image shows the generated harmonics, the middle image shows the measured laser beam spatial profile, and the graph on the right shows a lineout of the laser beam spatial profile. The units on the laser image and beam lineout are scaled to the dimensions of the laser focus in the gas cell rather than the image size on the CCD. Each image is the average of 10 laser shots.

Figure 2.5a plots the beam diameter in both 80 torr helium and vacuum as the foil position is varied. In helium, the width of the beam reaches a minimum near

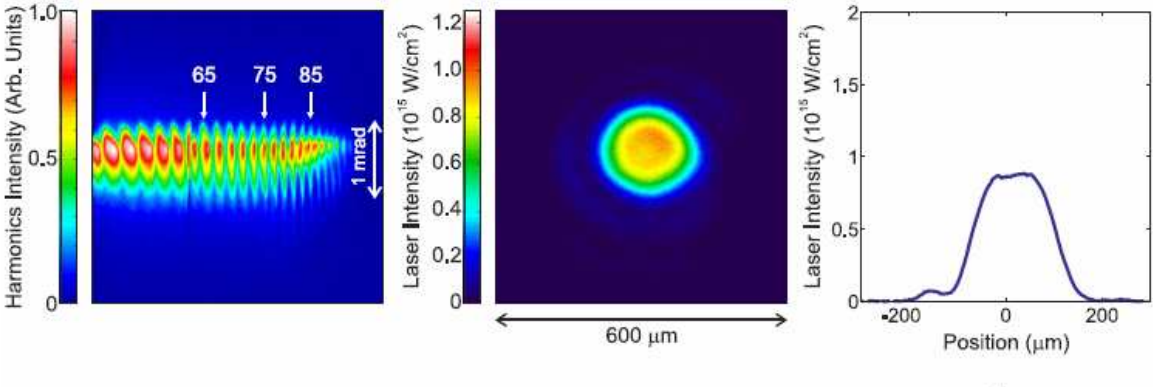

Figure 2.4 Harmonics (left), imaged laser beam (center), and beam lineout (right) for harmonics generated in 80 torr helium at the z=0 position, or where the beam focuses in vacuum.

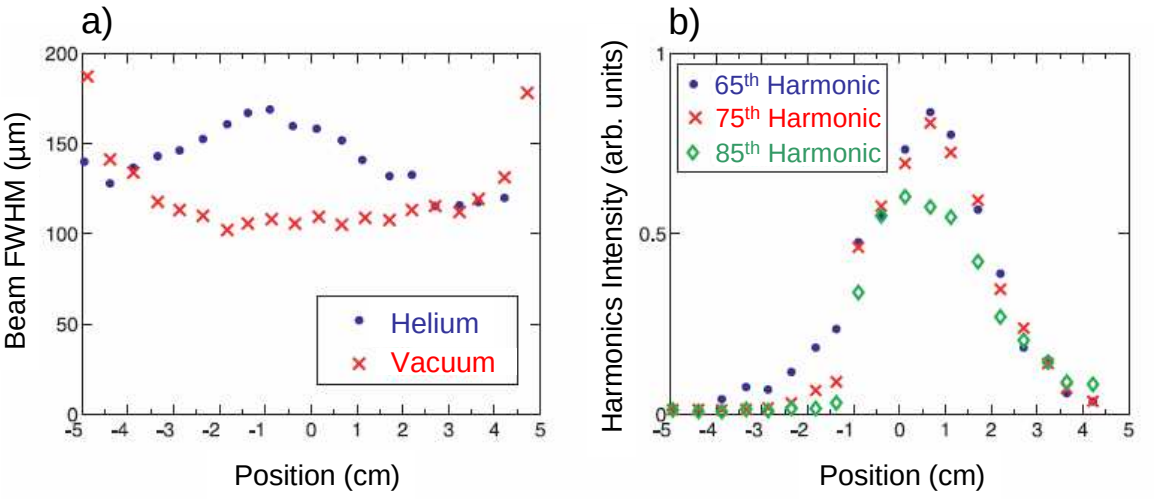

Figure 2.5 (a) Diameter of the laser as it exits from the gas cell, either filled with 80 Torr helium or evacuated. The best focus in the absence of gas occurs 100 cm after the focusing mirror. (b) The brightness of several harmonic orders as the foil position is varied.

z = -3 cm, widens to reach a maximum near z = 0 cm, and then narrows again to a second minimum at z = 4 cm. In vacuum the beam goes through a single focus, as would be expected. The z-position of the exit foil is measured relative to a location 100 cm from the focusing mirror, which is where the beam focuses in vacuum. Figure 2.5b, shows the intensity of several harmonic orders at the foil positions where the beam diameter in helium was measured. The best harmonic production is observed around z = 0.5 cm, where the laser in helium is changing from diverging to converging. Figure 2.6 compares intensity lineouts of the laser beam focused in helium and in vacuum. The beam propagating in vacuum shows a Gaussian-like profile, which reaches a single minimum width with maximum intensity at z = 0 cm. The beam propagating in helium exhibits the double focus discussed above, and a distinct flat-top radial profile from about z = -2 cm to z = 1.5 cm. Although not immediately apparent from the lineouts, the two curves correspond to similar total energies. (The intensity at wider radii is incident on a larger area, so in two dimensions the extra intensity in the wings of the profile in helium compensates for its lower on-axis intensity).

A flat-top profile was previously associated with laser self guiding and extended phase matching in neon [29,30]. Tosa *et al.* [29] calculated the radial intensity profile of a self-guided beam and predicted that it would exhibit a top-hat profile, owing to wavefront distortions from free electrons. Kim *et al.* [30] subsequently observed a radial intensity flattening in a single image produced for a laser that had traveled through a wide gas jet. The top-hat profile was attributed to defocusing of the laser by free electrons at inner radii. As the on-axis energy is defocused out to wider radii, it overlaps with the less intense outer portion of the laser beam still in the act of focusing. While this explanation is consistent with the radial intensity distribution observed and laterally broadened wave fronts, it was not at first obvious how this

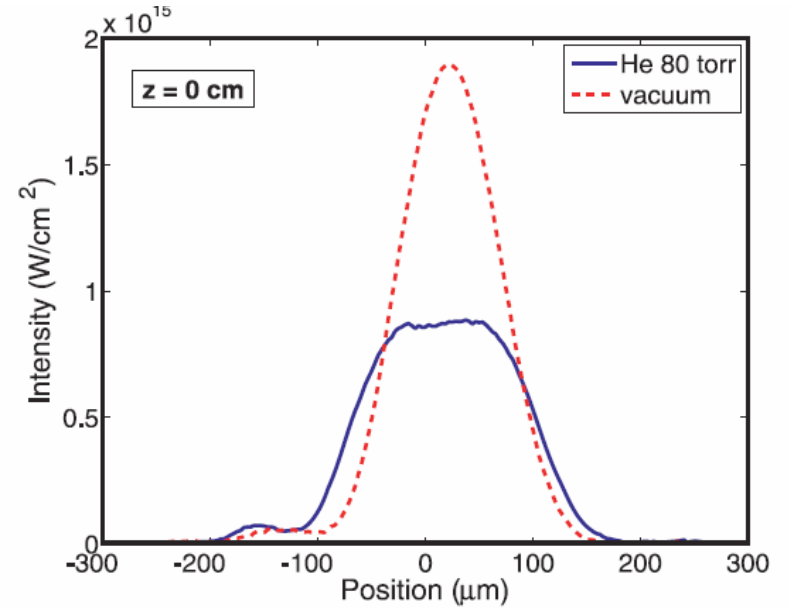

Figure 2.6 Lineouts of the laser focused in helium and in vacuum at the z = 0 cm position, or where the laser focuses in vacuum.

could offer good longitudinal phase matching for high-harmonic generation. It was also not obvious how this could cause a re-convergence of our beam to a second focus, as seen in the data. However, recent calculations indeed show that these behaviors arise from an interplay between the diffraction caused by the partially closed aperture and the dispersion caused by free electrons generated in the focus. The results appear to be consistent with the mechanisms described previously by Tosa, *et al.* [29].

2.4 Discussion

The double focusing observed in our laser beam as it interacts with helium is suggestive of Kerr-style self-focusing, or filamentation. Placing a partially closed aperture in the laser beam before the focusing mirror causes the observed laser focus to be smoother while at the same time dramatically increasing the high harmonic signal. This effect may support the idea of Kerr-style self-focusing in the sense that a

smoother beam will tend to favor the formation of a single filament rather than competing filaments. Nevertheless, the nonlinear index in 80 torr of helium is reported to be approximately 4×10^{-22} cm^2/W [22, 23], which predicts a critical power for filamentation [24] in excess of 2 TW. In contrast, the power used in our experiments was an order of magnitude less. Tosa and coworkers [29] also indicate that the Kerr nonlinearity should be inconsequential.

The development of a flat-top intensity profile in the laser focus is consistent with the predictions and observations of Tosa and Kim [29, 30]. However, our observation of double foci at first appeared to be unexpected within their description. The brightest harmonics are attained when the exit foil of the gas cell is positioned near the middle of the self-guiding region, where the beam diameter is largest. This region of extended phase matching occurs where the laser beam changes from diverging to converging between the two foci. This is opposite in character to a conventional laser focus, which changes from converging to diverging while accompanied by the Gouy shift (known to be deleterious to phase matching). The interpretation of the data is complicated by the fact that the CCD camera measures energy fluence rather than intensity (technically a mislabeling of Figures 2.4 and 2.5). Our measurement technique is therefore unable to distinguish whether the entire pulse in time develops the flattop profile as seen in the data, or whether different temporal portions of the pulse look spatially different. Recent calculations by Matt Turner in our research group have shown the unexpected result that both the flat-top intensity profile and the double foci in the laser beam can be explained as a combination of laser diffraction from a partially closed aperture and dispersion caused by free electrons in the laser focus. These findings confirm the explanation made by Tosa [29] that the Kerr effect is inconsequential.

Chapter 3

Description of Polarimeter and Procedures

3.1 Positioning System and Alignment

The major components of the polarimeter are the sample, the grating, and the microchannel-plate detector. The positioning system is made up of six motors, all controlled by a single computer, as seen in Figures 3.1 and 3.2. The sample sits above two concentric rotation stages. One varies the incident angle of the harmonic light on the sample. This provides measurements of sample reflectance as a function of angle. The other swings the entire detection system (grating and microchannel plate detector) through twice that angle, allowing detection of reflected light. A second pair of rotation stages sits beneath the grating: one to adjust the grating angle to measure different wavelengths of light and the other to separately adjust the angle of the microchannel plate to allow detection of diffracted light. A linear translation stage is used beneath the microchannel plate detector to focus the harmonic orders of interest onto the detector. The sample is also connected to a linear translation stage.

This allows the sample to be moved out of the beam to obtain incident intensity measurements of harmonics.

The microchannel plate detector needs to be kept at pressures lower than 10^{-5} torr while in operation to prevent arcing. The polarimeter positioning system is housed in a vacuum chamber of approximate dimensions 1.5 m×1 m×30 cm, however, which is difficult to pump down to the necessary pressures. To deal with this, we placed a small vacuum chamber (11.4 cm×11.4 cm×11.4 cm) inside the large vacuum chamber. This secondary vacuum chamber has its own turbo pump and a pinhole for the harmonics to enter. With differential pumping, this secondary chamber can reach base pressures lower than 10^{-6} torr while the large chamber is at 10^{-4} torr. The entire system can pump to the necessary pressures in less than 30 minutes without special cleaning procedures.

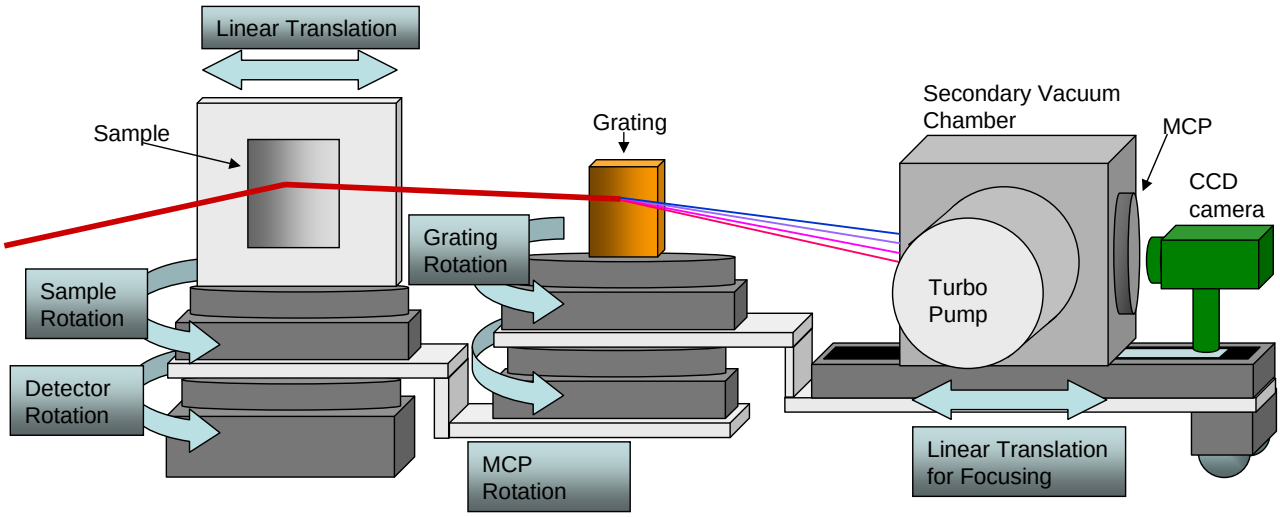

Figure 3.1 Polarimeter positioning system, side view

The positioning accuracy of the rotation stages (ThorLabs NanoRotator NR360S) is 3×10^{-4} degrees. However, on two of our rotation stages (detector rotation and

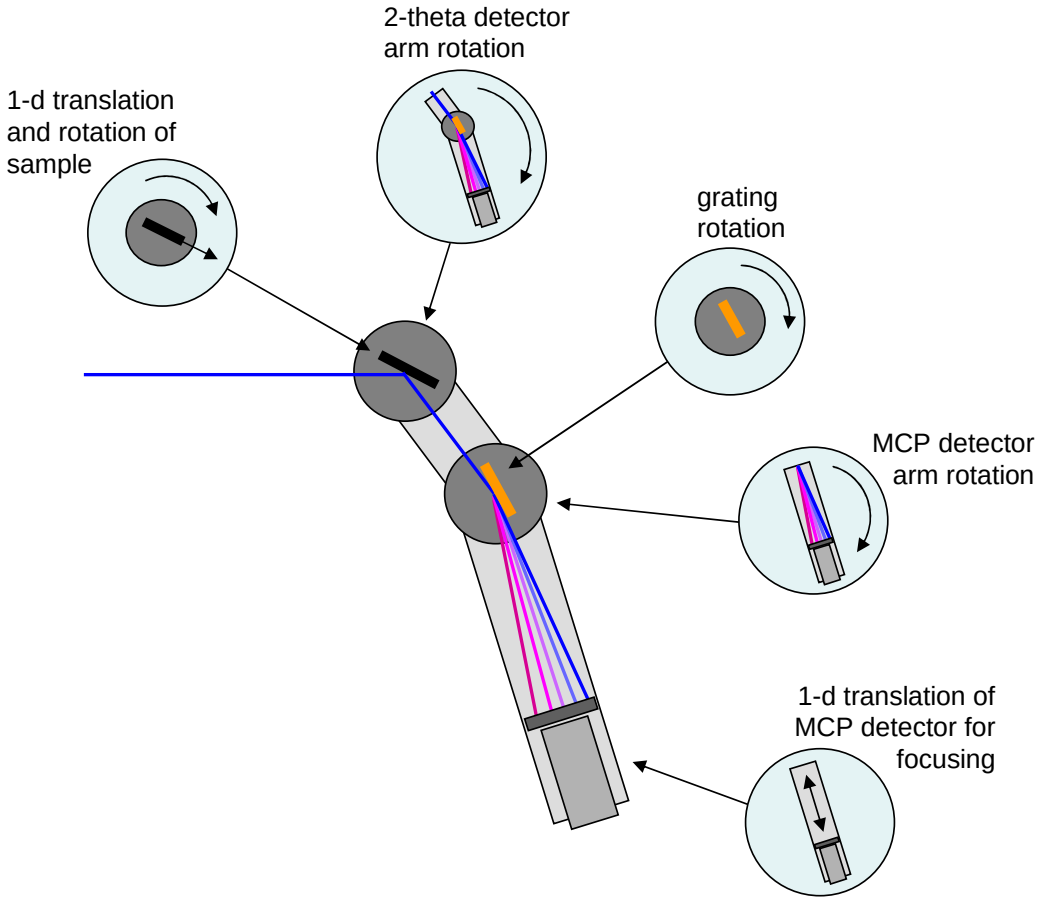

Figure 3.2 Polarimeter positioning system, top view

MCP rotation) we significantly exceed the torque limit of 23.1 N·cm. The major contributors to weight are the secondary vacuum chamber weighing 30 lbs and the turbo pump weighing 7 lbs. This weight is located at approximately 45 cm from the detector rotation stage and 30 cm from the MCP rotation stage. We placed wheels under the secondary vacuum chamber to help with the load, but the torque is still far above 23.1 N·cm. Because of this sizeable torque, these two motors only have a positioning accuracy of 1 degree. This is unacceptable. We must be able to position the reflected/diffracted harmonic beams to the same position on the MCP to within 1 mm using both motors in order to distinguish harmonic orders from each other. When considering the fairly large distances that the harmonic beams have to travel, the first motor must have positioning accuracy of 0.13 degrees, and the second motor must have positioning accuracy of 0.2 degrees. If we can position this well, we can use software to line up the harmonics to within 30 μm.

Our solution to this problem is to implement an in-situ alignment system using a HeNe 632.8 nm laser (refer to Figure 3.3). The laser enters the large vacuum chamber through a lens in a side port. A mirror on a solenoid can be moved into position while under vacuum, allowing the HeNe laser to propagate temporarily along the same path as the infrared laser. The HeNe laser focuses to a spot size of 1 mm on the diffraction grating. A small CCD camera views the HeNe laser spot on the diffraction grating surface.

Once the detector motor has been moved to a rough position, fine adjustments can be made to position the HeNe laser to the correct position on the diffraction grating. This procedure allows positioning accuracy of better than 0.11 degrees for the detector rotation stage. A similar procedure is employed to increase the accuracy of the MCP rotation stage. A CCD camera inside the small vacuum chamber images the microchannel plate. The same HeNe laser reflects zero order light off of the

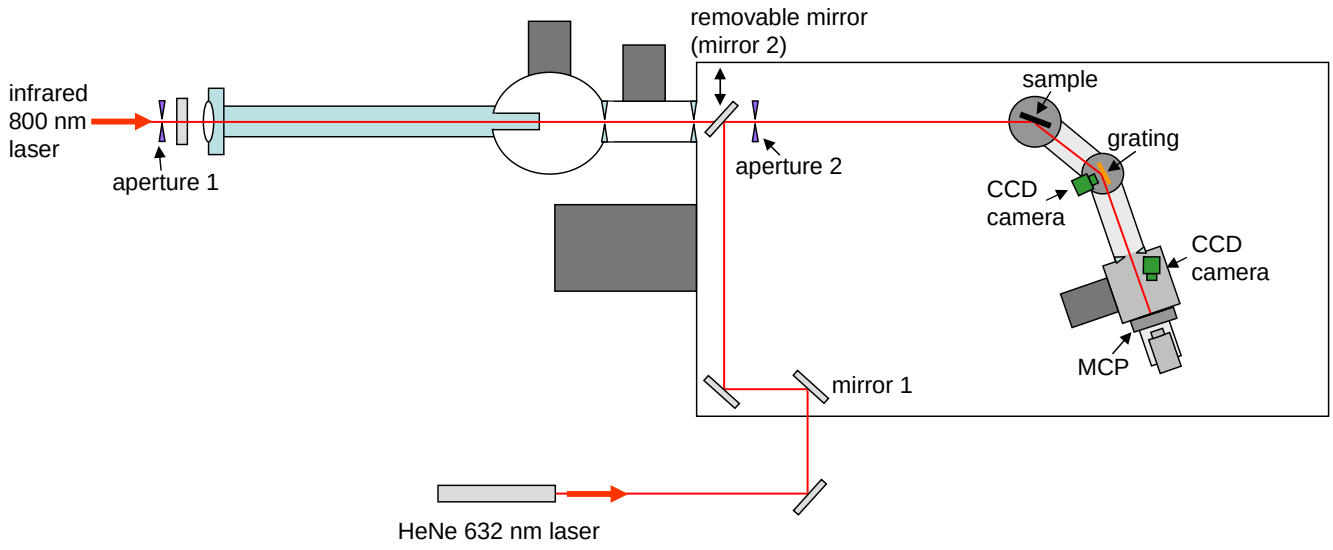

Figure 3.3 In-situ HeNe laser alignment system.

diffraction grating and enters the small vacuum chamber. By rotating the grating 3 degrees, we can image the HeNe laser on the MCP. The laser here is about 4 mm in diameter. Once the MCP motor has been moved to a rough position, fine adjustments can be made to position the laser to the correct position on the MCP. This allows positioning accuracy of better than 0.2 degrees for the MCP rotation stage.

The alignment procedure for the system is as follows (see Figure 3.4):

1. At low power, align the infrared laser with apertures 1 and 2.
2. Move the sample to 90 degrees and adjust the sample angle until it retroreflects the laser beam back through the apertures . A HeNe laser can also be used temporarily in place of the infrared laser system.
3. Turn on the solenoid that inserts the HeNe mirror (mirror 2) into the laser path. Align the HeNe laser along the same path as the infrared laser by aligning with aperture 2 with mirror 1 and adjusting mirror 2 until the HeNe laser beam retroreflects from the sample.
4. Move the sample out of the laser path with the linear sample stage.
5. To align the detector arm, adjust the detector angle until the HeNe laser is centered on the grating.

6. Move the sample back into the beam with the linear sample stage. Because the detector angle was adjusted in the previous step, the sample angle will now be slightly off (the sample motor is on top of the detector motor, so moving the detector motor also moves the sample). Adjust the sample angle again so that it is retroreflecting the HeNe laser. This angle is defined as the sample 90-degree position.

7. Move the sample angle to 0 degrees. Align the sample z-position by adjusting the micrometer on the sample stage until the sample is cutting off half of the HeNe beam.

8. The vacuum gauge on the secondary vacuum chamber causes a physical constraint such that the MCP arm cannot be moved to 0 degrees at the same time that the detector arm is moved to 0 degrees. To align the MCP arm, move the detector angle to any angle greater than 10 degrees. Move the MCP arm angle to 0 degrees and adjust until the legs line up.

9. To align the grating angle, move the sample angle to half of what the detector angle is. This reflects the HeNe laser onto the grating. Move the grating angle to 0 degrees and adjust this angle until the grating is cutting off half of the HeNe beam.

10. The grating and MCP arm angles are now both at 0 degrees. To see harmonics, the grating should be moved to approximately 8 degrees and the MCP arm should be moved to approximately 19 degrees. These angles can be adjusted while viewing harmonics to view desired harmonic orders.

11. To prepare the positioning system for an incident intensity measurement, which is usually the first step in a reflectance scan, move the detector angle to 0 degrees, the sample angle to 90 degrees, and move the sample out of the beam with the linear sample stage.

We found that the positioning system was accurate enough for us to distinguish harmonic orders from each other. A typical position difference between two harmonic measurements was about 0.3 mm (see Figure 8). However, because of the sharpness of the peaks, we are able to use software to shift the data to align the harmonics on top of each other to within 30 μm. Using both of these techniques, we are able to obtain a spectral resolution ($\lambda/\Delta\lambda$) of 180 (discussed in section 3.4).

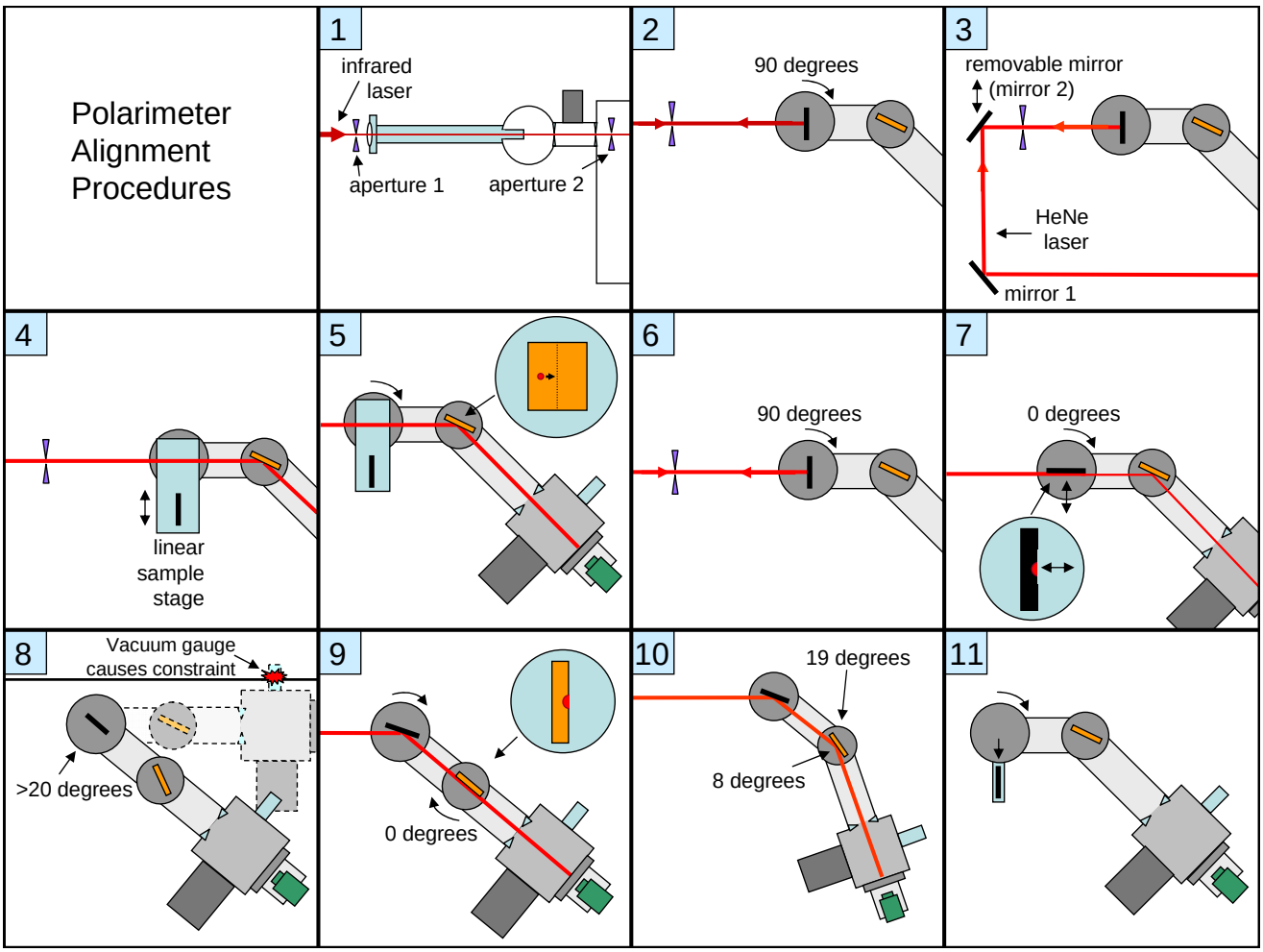

Figure 3.4 Schematic of steps for aligning the polarimeter.

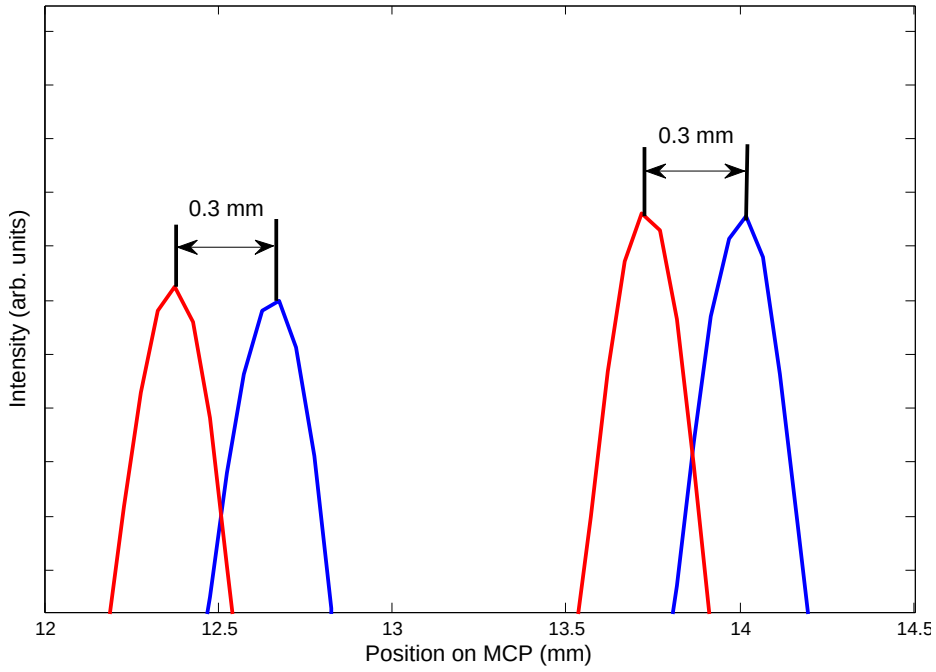

Figure 3.5 Two measurements of the 41st and 43rd harmonics to show positioning repeatability. Because of the sharpness of the peaks, positioning accuracy can be combined with electronic means to align harmonics on top of each other to within 30 μm.

3.2 Detector Setup

The detector consists of a stacked microchannel plate pair coupled to a phosphor screen. The front plate is connected to ground and the back plate is held at 1100-1600 V. The phosphor screen is powered with 5200 V. A visible light CCD camera captures the image on the phosphor screen and is read by a computer.

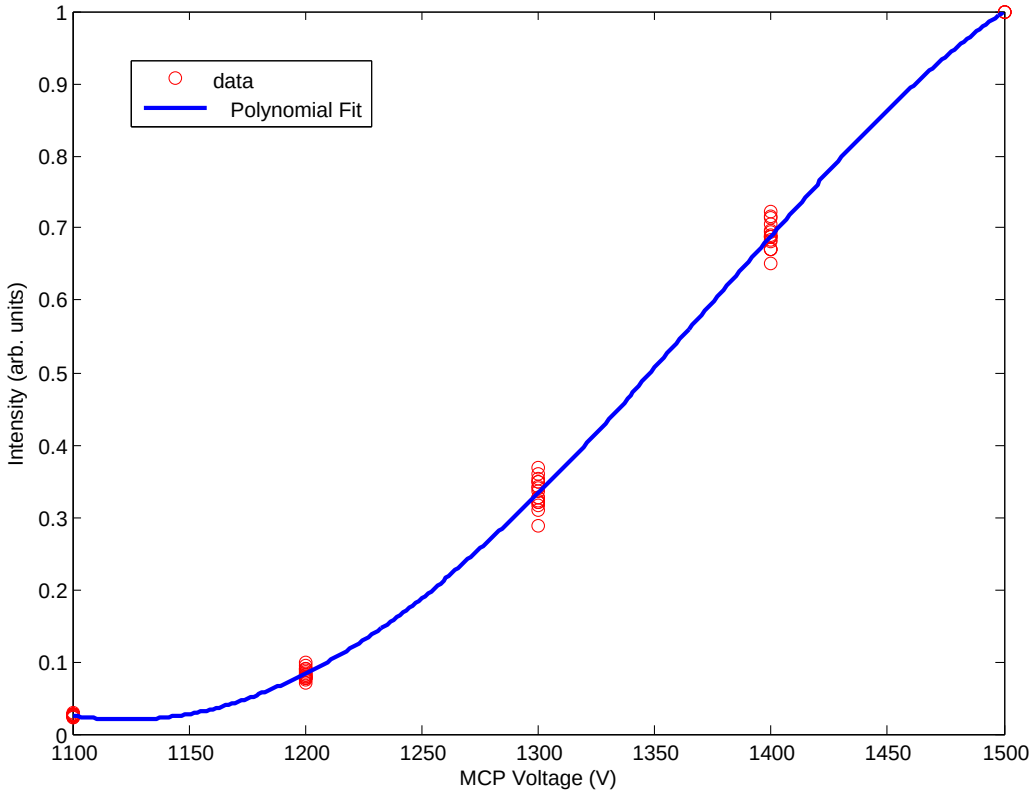

Figure 3.6 Characterization of the microchannel plate response as the plate voltage is increased. Also plotted is a polynomial fit of the response.

In order to increase the dynamic range of our detector for the sake of low reflectance measurements, we found it necessary to increase the voltage on the second plate of the microchannel plate detector as the signal decreased. This process is characteristically nonlinear. To describe this nonlinearity, we dimmed incident harmonics by lowering the gas pressure until they were barely visible with the MCP held

at 1100 V. We then increased the voltage while keeping gas pressure constant and averaging over 100 laser shots. This characterization along with a polynomial fit is depicted in Figure 3.6.

This method of increasing our dynamic range is characteristically flawed. The response of the microchannel plate is possibly slightly different for each wavelength of light incident on it. Also, as the plates age, they may change their response. A possible solution to this problem will be discussed in section 4.5.

3.3 Determination of Orders

To determine the wavelength of each harmonic, we placed a 0.2 μm aluminum filter on a solenoid in the vacuum chamber so that it could be moved into and out of the beam before the sample. The calculated transmission of the 0.2 μm aluminum filter is shown in Figure 3.7 [7].

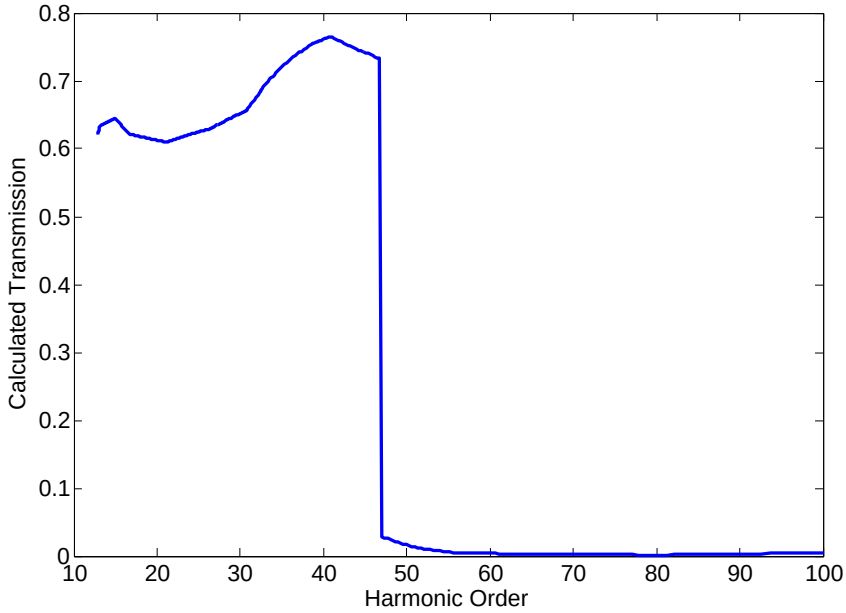

Figure 3.7 Transmission of a 0.2 μm aluminum filter calculated from optical constants.

The aluminum edge transmits harmonics of orders 45 and below, but not harmonic orders 47 and above. By moving the filter into the beam while observing harmonics, we can quickly see which is the 45th order. From there we simply count to find the rest of the harmonic orders (see Figure 3.8).

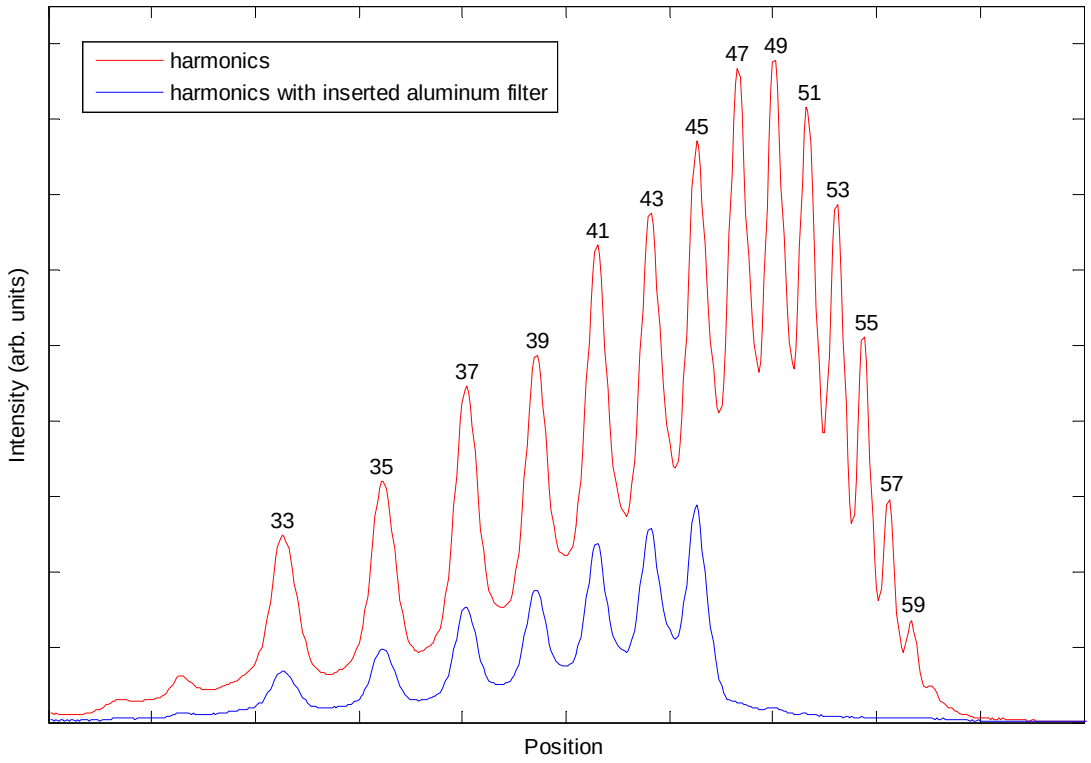

Figure 3.8 Harmonics measured with and without inserted aluminum filter.

3.4 Spectral Resolution

Our polarimeter's spectrometer is made up of a focusing diffraction grating. We do not employ a slit because the microchannel plate detector has spatial resolution, so each pixel is an effective slit. I developed a simple ray-tracing program to characterize the defocusing of the harmonics at the detector due to abberations in the imaging

system. The program traces rays from a 100 μm extended light source to a 2 m radius, 1200 lines/mm, 2 cm grating at an incident angle of 4 degrees, 1.5 m away from the source (see Figure 3.9), the same setup that exists in our polarimeter. The harmonics are diffracted and focused in one dimension by the grating. They are then allowed to propagate for 1 m. The location of the focusing (or image distance) is given by

$$\frac{\sin^2\theta_1}{d_o} + \frac{\sin^2\theta_2}{d_i} = \frac{\sin\theta_1 + \sin\theta_2}{R} \tag{3.1}$$

where θ_1 is the incident angle of the light on the grating measured from grazing, θ_2 is the diffracted angle of the light measured from grazing, d_o is the object distance, d_i is the image distance, and R is the radius of curvature of the focusing diffraction grating [31]. Both this equation and our program gave a focusing location of about 33 cm for the 45th harmonic. This confirmed the accuracy of our program.

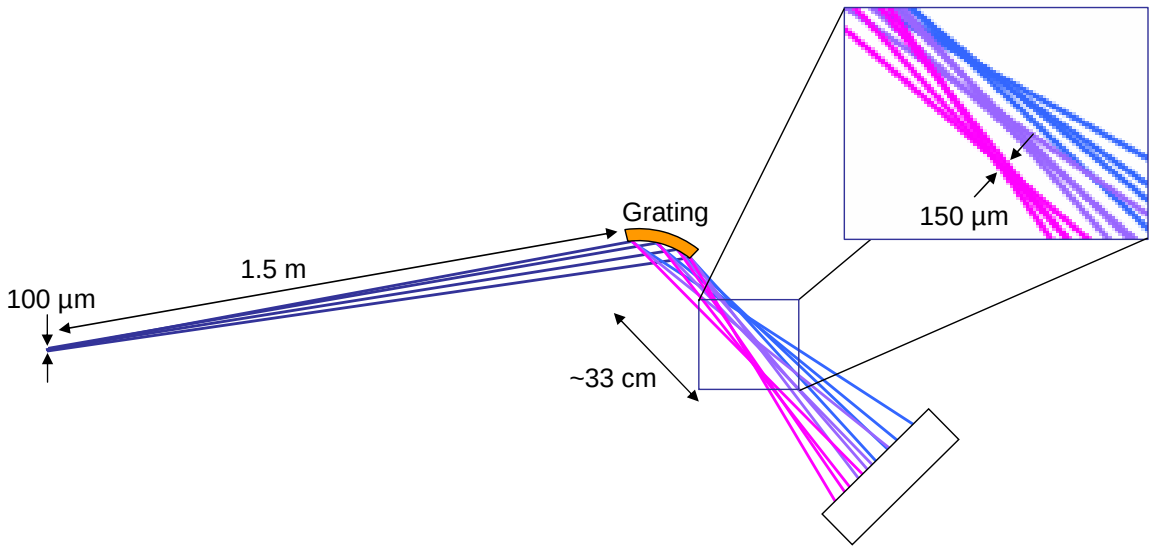

Figure 3.9 Schematic of setup for ray-tracing program to determine spectral resolution.

Figure 3.10 shows the rays of seven harmonic orders about 33 cm after the grating as calculated by our program. Each harmonic order focuses to a spot size of

about 150 μm. However, each harmonic order focuses to a different location after the grating. This means that at our detector, at most one harmonic order will be in focus. However, Figure 3.10 also shows that in a certain region, none of the harmonic beams overlap. This means that at best focus the signal should go to zero in between each harmonic order. Yet, we do not see this in our measurements, as can be seen in Figure 3.11. Figure 3.12 shows a fit of the harmonics where each harmonic was fit to a gaussian. Overlap of the harmonic beams accounts for some of the signal in between harmonics, but not all of it.

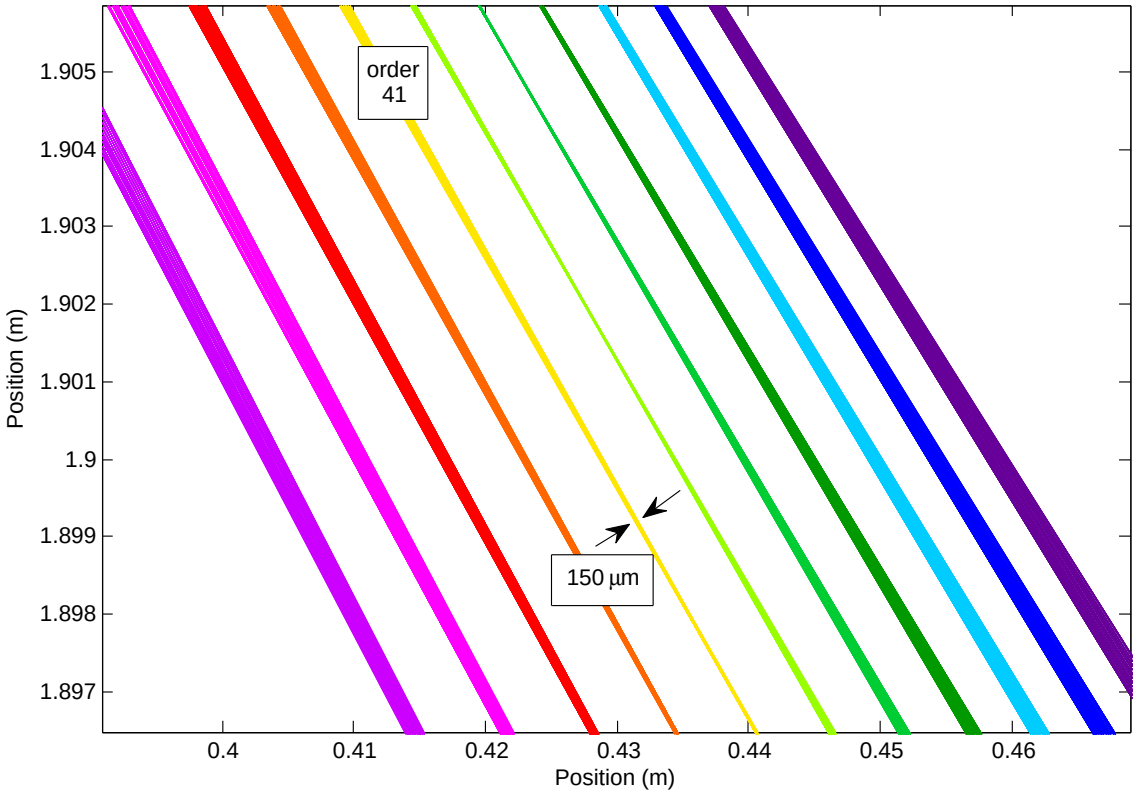

Figure 3.10 Widths of seven harmonics determined with ray tracing, assuming a source size of 100 μm and a beam size at the grating of 2 cm.

The fact that signal does not go to zero in between harmonic orders tells us that there is spectrum present in between harmonic orders. The infrared laser that

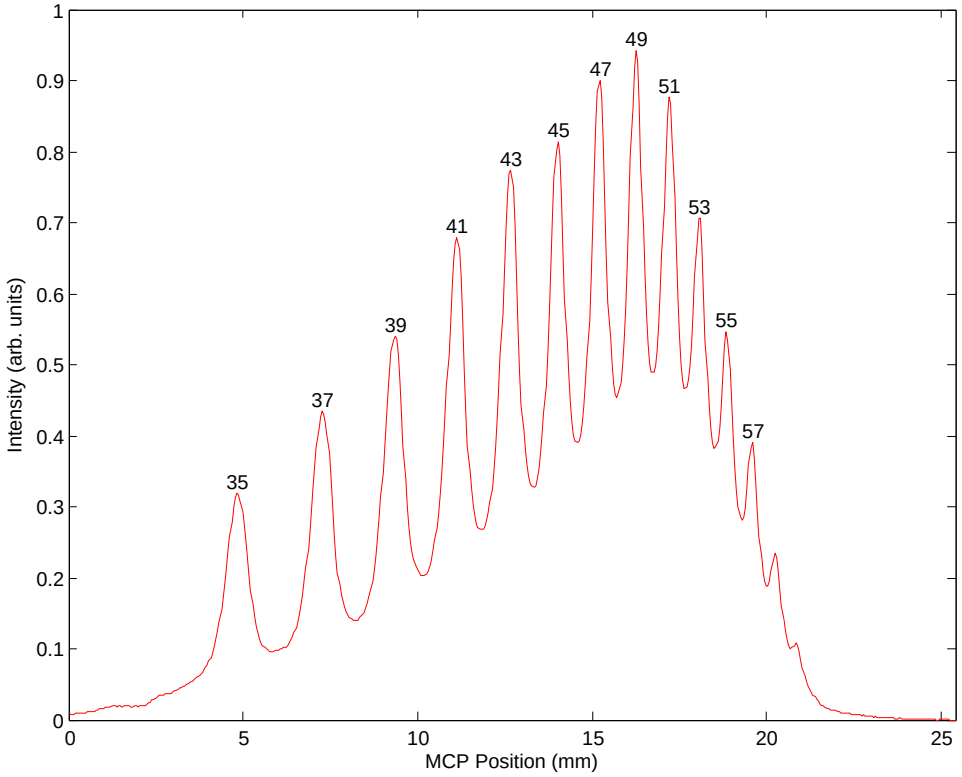

Figure 3.11 Lineout of incident harmonics. The sharpness of the harmonic peaks confirms that non-zero signal between harmonics is not due to defocusing.

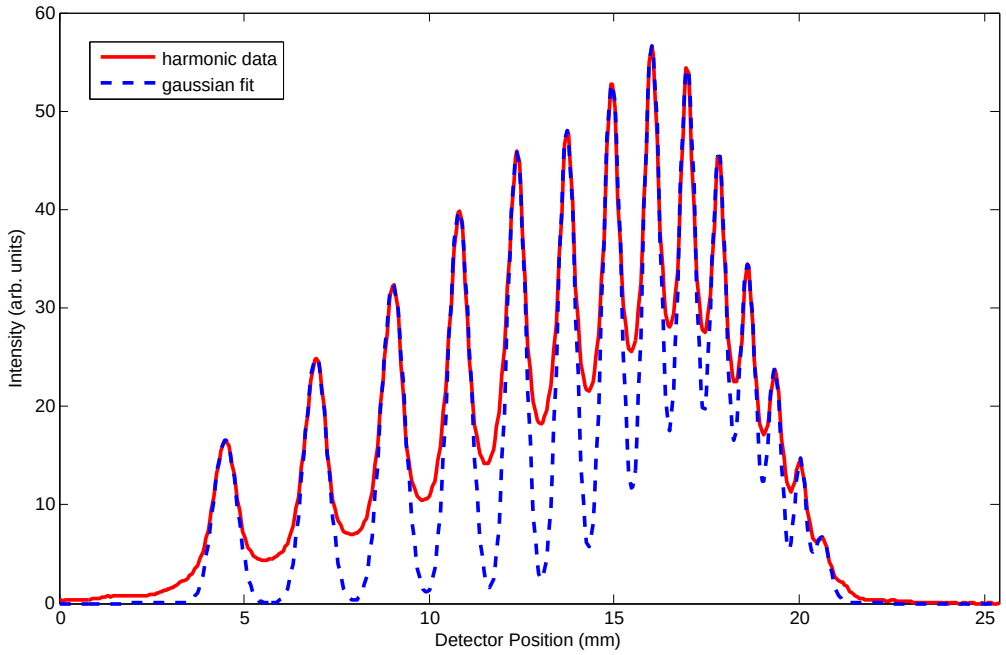

Figure 3.12 Lineout of incident harmonics along with a gaussian fit of each harmonic. This shows that harmonic beam overlap does not account for all non-zero signal in between harmonics.

generates harmonics has a frequency spread of 35 nm (FWHM) that will result in harmonics with frequency spread, but this only accounts for spread on the order of 1 nm. This indicates we actually have a broadband source with an intensity modulation on top of it. This is not due merely to blurring in the imaging system since the harmonic peaks are relatively sharp. This suggests that there are multiple regimes in the harmonic-generation process, one that creates sharp orders, and another that creates a broadband of EUV wavelengths at a lower intensity. The existence of wavelengths of light in between harmonic orders is good in that we can get all wavelengths of light.

The width of a typical harmonic peak is about 150 μm, which matches very well with that predicted by ray tracing. Since harmonics can be lined up with a combination of positioning system and software to 30 μm, blurring due to abberations in the grating image will be the limiting factor in the spectral resolution. As in Figure 3.11, there is 8.8 mm between the 39th harmonic and the 53rd harmonic. This represents a change of 5.4 nm in wavelength. Thus we see a change in wavelength of about 0.62 nm for every millimeter on our detector. If we can resolve blurring of our peaks up to 150 μm, we can resolve a change in wavelength of 0.092 nm. This gives a spectral resolution of about 184.

3.5 Source Stability

The stability of our high harmonic source is very important in performing accurate polarimetry measurements. Reflectance measurements are defined as reflected signal divided by incident signal. Accordingly, variation in incident signal will affect the accuracy and repeatability of reflectance measurements. There are many factors to consider when determining the stability of the high harmonic source. For example,

one of the main causes in variation of harmonic signal is that small variations in pump laser energy translate to large variations in harmonic output because of the significant nonlinearity. Also, gas pressure variations, optic damage over time, and laser energy drift may affect the harmonic output over the course of a run. Short term stability, in other words stability from laser shot to laser shot, in high harmonics is not good. Figure 3.13 shows that harmonics can vary from shot to shot by as much as 37%.

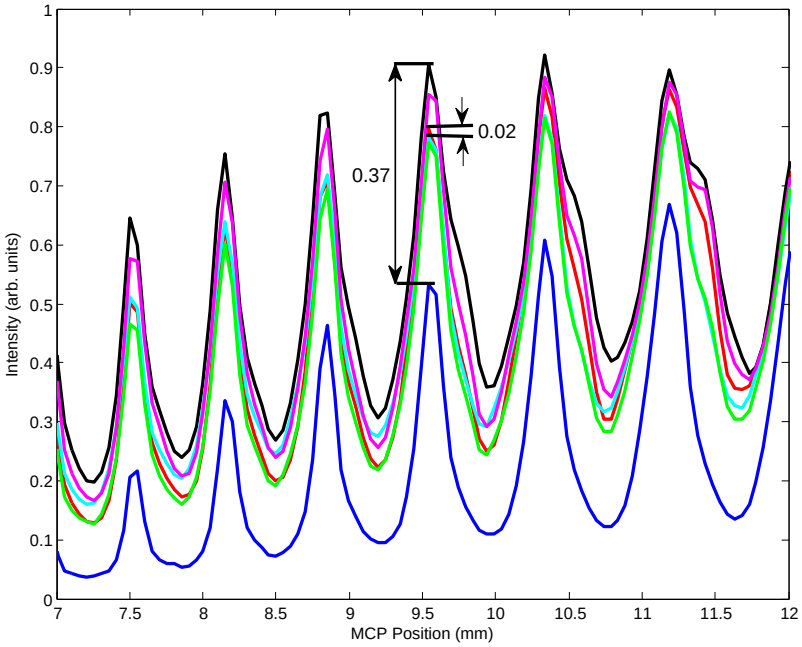

Figure 3.13 Short term, or shot to shot, stability of high harmonic source. Intensity of a single harmonic varies by as much as 37% and as little as 2%.

Because harmonics are unstable shot to shot, we average 100 shots (10 seconds) for each data file taken. The repeatability between harmonics averaged over 100 shots is much better, as seen in Figure 3.14. Variation is on the order of 7%.

Another type of stability is long term, or variation over the course of a run. Figure 3.15 shows three incident intensity measurements taken over the course of a run. I_0(t=0) was taken at the beginning of the run, I_0(t=10 min) was taken halfway

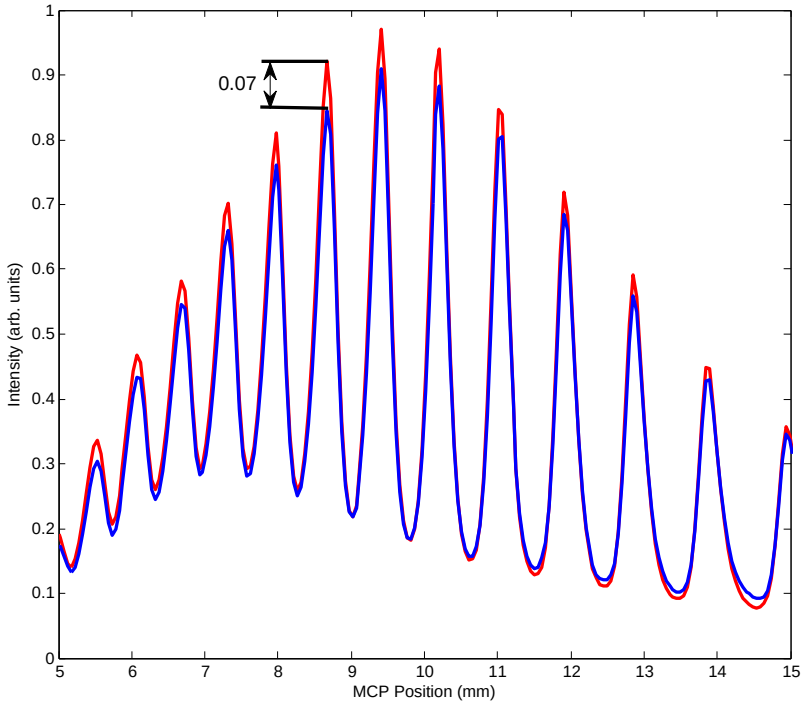

Figure 3.14 Stability of harmonics averaged over 100 shots, or 10 seconds. Variation is on the order of 7%.

through the run, and I_0(t=20 min) was taken at the end of the run. The run lasted approximately 20 minutes. The variation was on the order of 12%. There is a general trend of decreasing intensity over the course of the run, though it seems that some harmonics are varying independently of others.

Stability over 100 shots is on the order of 7% and long term stability is on the order of 12%. Long term drift can be corrected for with frequent re-measurements of the incident EUV radiation during a scan. Thus error in reflectance measurements will be between 7% and 17% (adding in quadrature) depending on how often incident intensity measurements are taken.

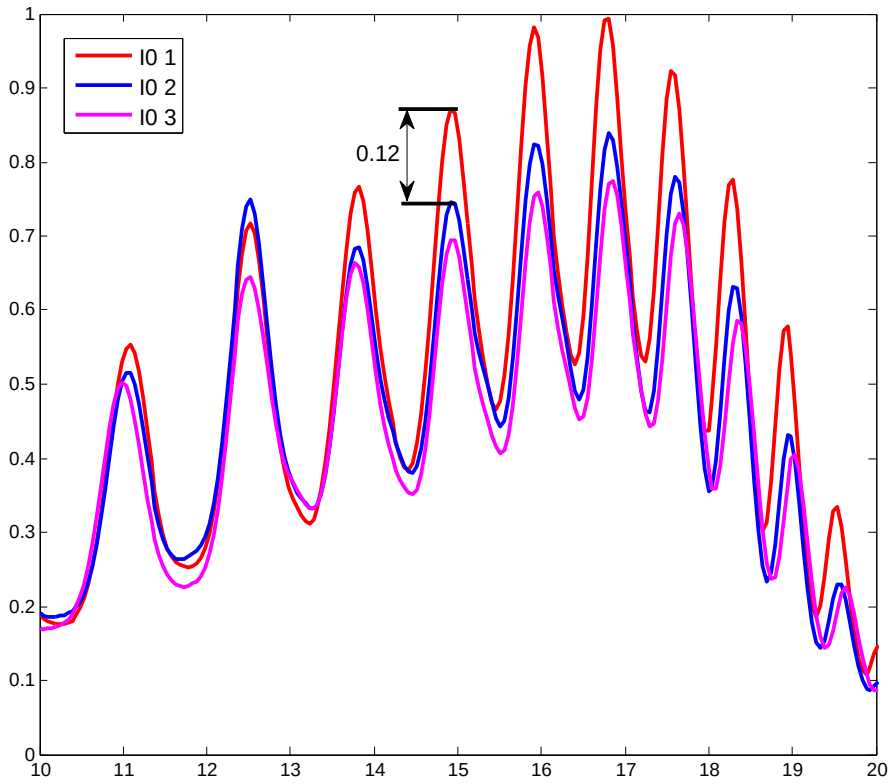

Figure 3.15 Stability over the course of a run. $I_0 1$ was taken at the beginning of the run, $I_0 2$ was taken halfway through the run, and $I_0 3$ was taken at the end of a run (a total of about 20 minutes). Variation is on the order of 12%.

Chapter 4

Reflectance Measurements

4.1 Sample

We used a silicon substrate with a thermally oxidized layer as a test sample to characterize our instrument. Prof. Allred performed spectroscopic ellipsometry on the sample and found the thickness to be 27.4 nm$\pm$0.2 nm [32]. This sample is a good reference surface for characterizing the accuracy of the polarimeter at wavelengths from 8 nm to 20 nm. This is because the thickness is such that interference in reflected light from the front and back surfaces of the silicon dioxide layer create fluctuations in reflection as the sample angle is rotated. These fluctuations are commonly referred to as interference fringes, and they make it easy to compare data taken with our EUV polarimeter with data taken with another source, such as the Advanced Light Source. Also, this sample has interference fringes near Brewster's angle ($\sim$45°), which allows us to see significant differences in reflection at s- and p-polarizations. This makes it easy to see the effect of polarization on reflectance. Silicon dioxide on silicon is also a good reference sample because it is stable in air for long periods of time, the two surfaces of the oxide can be exceptionally smooth, and the oxide can

be quite uniform.

4.2 Reflectance Measurements and Repeatability

High harmonics for these measurements were produced in 57 torr of neon gas. An aperture was placed immediately before the focusing lens at an optimal diameter of 1.1 cm. The gas cell was placed so that the exit foil was positioned 100 cm from the focusing lens. Reflectance measurements were taken at multiple wavelengths simultaneously. All measurements were averaged over 100 shots. Reflected signal was determined by making a lineout of the harmonics at each angle by averaging in the y-direction over the area shown in Figure 4.1. Harmonic orders were then determined using the method discussed in section 3.3. The maximum value of each harmonic was used for the reflected signal for that wavelength at each specific sample angle. Dark current is determined by averaging over an area away from the harmonics (also shown in Figure 4.1). The advantage of measuring dark current in this way is that it is taken simultaneously with reflected signal. It thus takes into account angular dependence and any other unknown that may affect the dark current at different points in the run. Incident intensity measurements were taken at three different times during the run, at the beginning, middle, and end. For this first iteration, we merely averaged the three incident measurements to get the incident signal for each harmonic order. S- and p-polarizations were found to reflect from the EUV grating slightly differently (see Figure 4.2), so each reflectance measurement was normalized using the incident measurement of the same polarization. The normalization algorithm followed the following format:

$$R = \frac{R_s - D_s}{I_s - D_s} \tag{4.1}$$

where R is the reflectance, R_s is the reflected signal, D_s is the dark signal, and I_s is the incident signal.

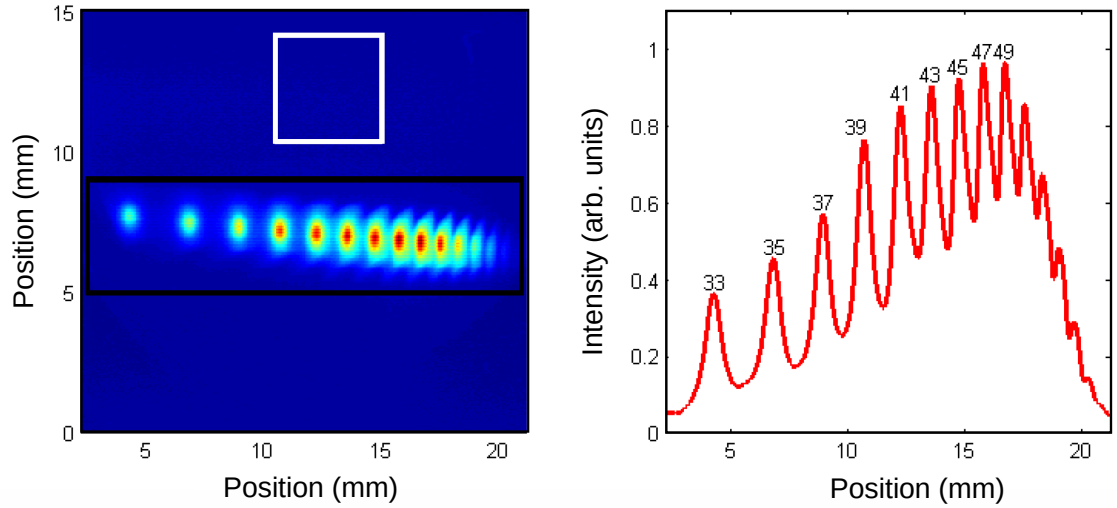

Figure 4.1 Harmonics (left) and lineout (right) at a sample angle of 10°. The black box in the left figure shows where harmonics are averaged in the y-direction to make the lineout. The white box in the left figure above the harmonics shows the area that is averaged to determine dark current.

Reflectance measurements were taken on three separate days in order to show repeatability. Figures 4.3-4.5 show these three measurements of reflectance at s- and p-polarizations for three representative wavelengths: 16.3 nm, 18.6 nm, and 22.9 nm. Repeatability was shown to be within the error of our source stability. We also found that we were able to measure reflectances as low as 0.2%.

4.3 Data Comparison with the Advanced Light Source

Reflectance was measured from the same sample by the Allred-Turley group at the Advanced Light Source at Lawrence Berkeley National Labs. This data is useful to compare with data taken with BYU's EUV polarimeter because the ALS is a standard

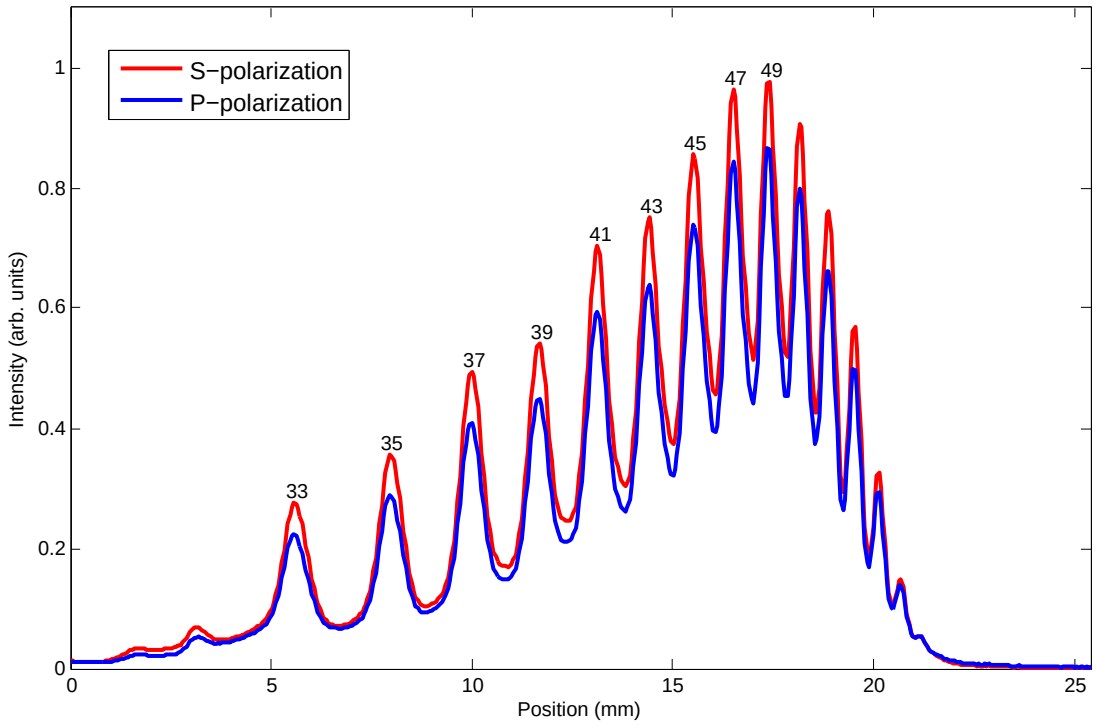

Figure 4.2 S- and p-polarized harmonics reflected slightly differently from the EUV grating. Accordingly, each reflectance measurement was normalized using the incident measurement of the same polarization.

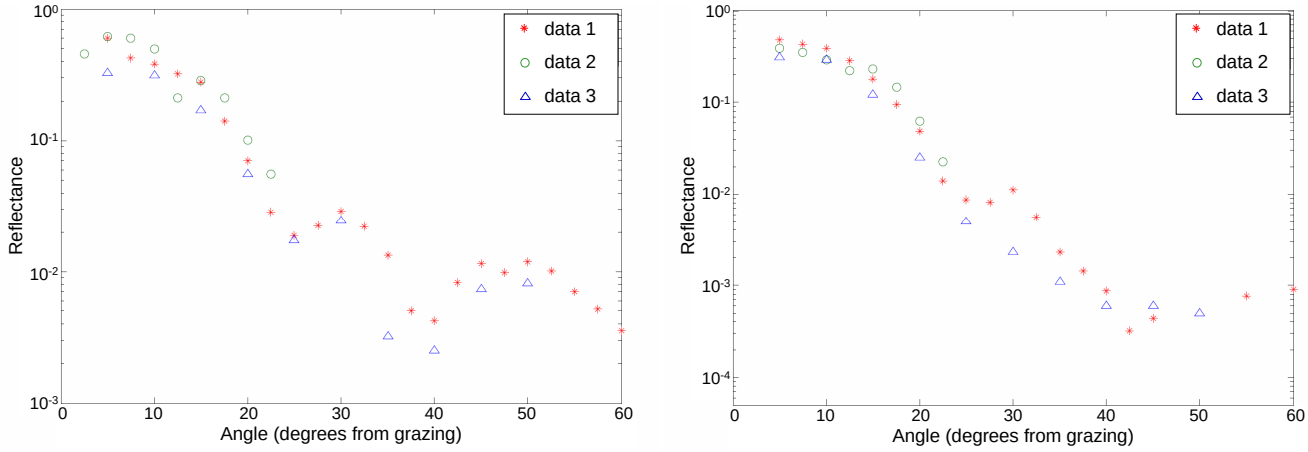

Figure 4.3 Comparison of three reflectance measurements made with BYU polarimeter at q=49 (λ=16.3 nm) with s-polarized light (left) and p-polarized light (right).

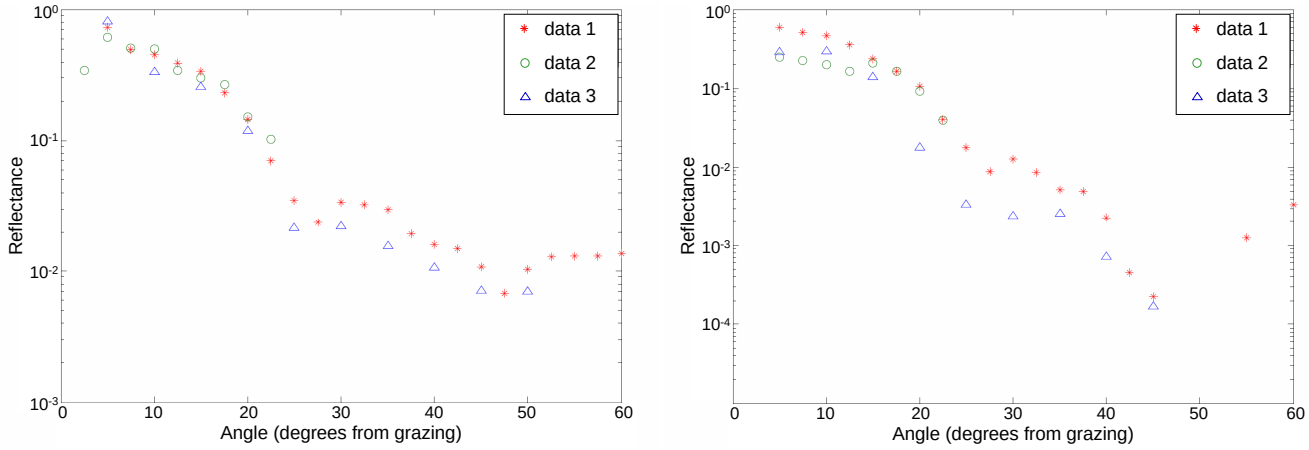

Figure 4.4 Comparison of three reflectance measurements made with BYU polarimeter at q=43 (λ=18.6 nm) with s-polarized light (left) and p-polarized light (right).

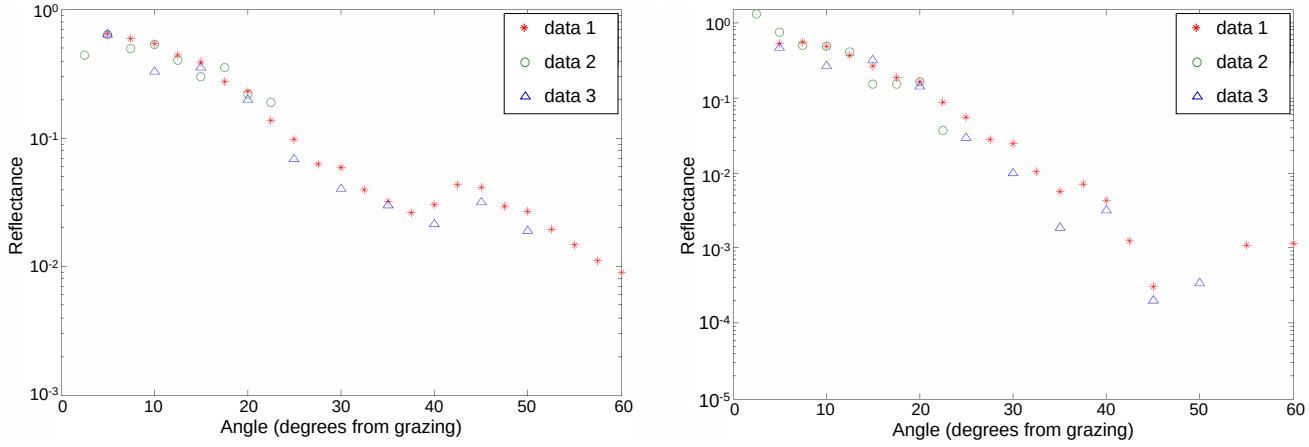

Figure 4.5 Comparison of three reflectance measurements made with BYU polarimeter at q=35 (λ=22.9 nm) with s-polarized light (left) and p-polarized light (right).

facility for measuring reflectance in the EUV. EUV light from the ALS is naturally polarized at 90% s- and 10% p-polarization by intensity. In order to prepare our data for comparison, we multiplied data measured with s-polarized light by 0.9 and added it to data measured with p-polarized light by 0.1 for each wavelength. Comparisons of these two measurements are shown in Figure 4.6. Because our three sets of data were shown to be similar in the previous section, we have only plotted here data set 1.

Data between 5 and 27.5 degrees agrees very well with data taken at the ALS. Also, interference fringes in both data sets match very well. After 27.5 degrees, the BYU polarimeter data is consistently higher. This consistent discrepancy could be explained if our compensation for the microchannel plate nonlinearity is incorrect at high plate voltages, which are necessary when signal is low.

4.4 Summary and Conclusions

We have developed a high-order harmonic source that represents a high-flux source of EUV light that has a wide wavelength range in the EUV, and has easily rotatable linear polarization. We have used the harmonics to construct an EUV polarimeter which employs laser-generated high-order harmonics as an EUV source. This polarimeter represents a useful research tool for the EUV thin-film research group and will facilitate our understanding of materials for use in EUV optics employed in varied applications. Polarization-sensitive measurements will enable better procedures for determining optical constants in the EUV. Our spectrometer has good spectral resolution, and the harmonics provide an excellent broadband EUV source. We have shown that by averaging data over 10 seconds we can maintain source stability of 7%. We have constructed a versatile positioning system that places harmonics on the microchannel plate detector with an accuracy of 0.3 mm. We have demonstrated that

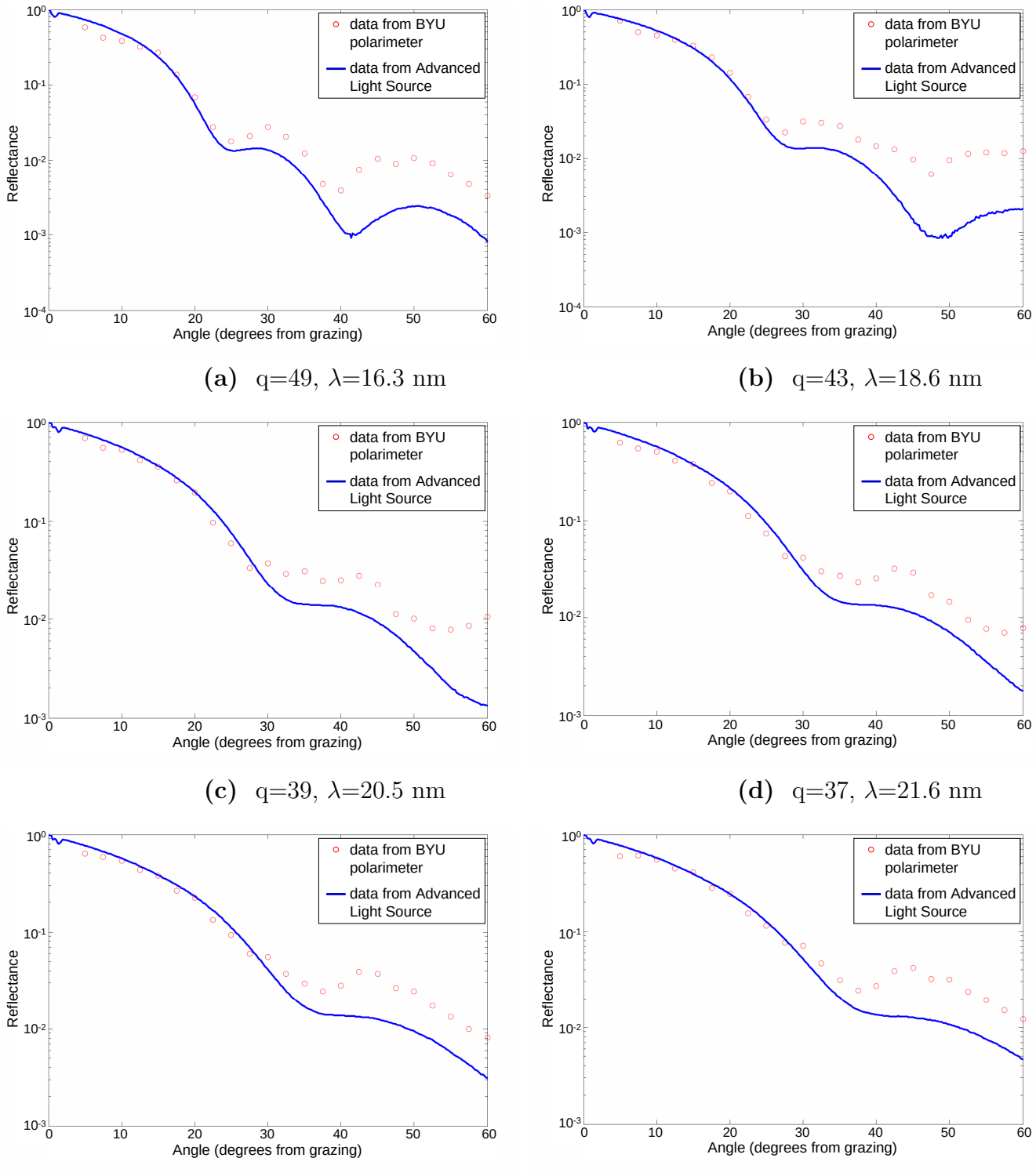

(a) q=49, λ=16.3 nm

(b) q=43, λ=18.6 nm

(c) q=39, λ=20.5 nm

(d) q=37, λ=21.6 nm

(e) q=35, λ=22.9 nm

(f) q=33, λ=24.2 nm

Figure 4.6 Reflectance measurements made with BYU polarimeter compared with measurements made at Beamline 6.3.2 of the Advanced Light Source.

reflectance data as low as 0.2% can be taken at EUV wavelengths and that this data is repeatable to within the error of our source stability. We have compared this reflectance data to data taken from the same sample at Beamline 6.3.2 at the Advanced Light Source. This data agrees well from 0 to ∼30 degrees, and the locations of the interference fringes also agree. Data at angles higher than 30 degrees are consistently higher than ALS data. This discrepancy may stem from nonlinearity in the MCP, which we will investigate in the future.

4.5 Future Work

After taking the first data set with the new polarimeter, we have identified several areas for improving instrument performance. Compensation for the nonlinearity of the microchannel plate will be one of the first things we will address. One solution to this problem is to create a controlled harmonic attenuator out of a second gas cell, similar to work by Christensen discussed in section 2.2. Absorption of each harmonic order through a gas could be characterized, then gas pressure could be increased or decreased to control photon flux on the MCP in a known way to avoid changing plate voltage.

A second problem we encountered was instability of our laser source. A method to improve this stability was implemented by Sutherland [18] and could be easily implemented in our work. Sutherland picked off a piece of the infrared laser before harmonic production and reflected it onto the exterior of the MCP phosphor screen in an unused region. This made it possible to record the laser energy inside the image that captured the high harmonic signal. As data was taken, it was binned so that only frames where the incident laser beam was within a specified energy range would be included. In this way, incident harmonic signal was controlled to be within

a certain range. Our setup is slightly more complicated than Sutherland's, in that our MCP detector is not in a fixed location, but we can implement the same control technique by sending a piece of the infrared laser down a fiber that would guide it to the detector.

Two more areas for future work are not solutions to problems, but conveniences that will make our polarimeter user friendly. First, we will complete automation of the positioning system using LabView programming. This programming is already underway and will not only make the polarimeter easy to use, but will decrease the time it takes to perform a run. This will decrease the possibility that long-term drift in harmonic output will affect reflectance measurements. Also, we have been working on replacing the HeNe laser alignment system with magnetic position encoders. This will also decrease the time needed to perform a run and will decrease the amount of human error incurred.

Bibliography

[1] B. Sandel, "IMAGE extreme ultraviolet imaged," http://euv.lpl.arizona.edu/euv/ (Accessed May 21, 2007).

[2] S. Lunt, "Determining the indices of refraction of reactively sputtered uranium dioxide thin films from 46 to 584 angstroms," Master's Thesis (Brigham Young University, Provo, UT, 2002).

[3] M. Urry, "Determining optical constants of uranium nitride thin films in the extreme ultraviolet (1.6-35 nm)," Senior Thesis (Brigham Young University, Provo, UT, 2003).

[4] J. Johnson, D. Allred, R. S. Turley, W. Evans, and R. Sandberg, "Thorium-Based Thin Films as Highly Reflective Mirrors in the EUV," Mater. Res. Soc. Symp. Proc. **893,** 207–214 (2006).

[5] N. Brimhall, A. Grigg, R. S. Turley, and D. Allred, "Thorium-based thin films in the extreme ultraviolet," Proc. of SPIE **6317,** 1–8 (2006).

[6] G. Acosta, Ph.D. dissertation (Brigham Young University, Provo, UT, 2007).

[7] B. L. Henke, E. M. Gullikson, and J. C. Davis, "X-ray interactions: photoabsorption, scattering, transmission, and reflection at E=50-30000 eV, Z=1-92," Atomic Data and Nuclear Data Tables **54,** 181–342 (1993).

[8] D. Allred, G. Acosta, N. Farnsworth-Brimhall, and R. S. Turley, "Simultaneous Reflection and Transmission Measurements from Coated Diodes to Determine the Optical Constants of Thin Films in the Extreme Ultraviolet," 49th Annual Technical Conference Proceedings, Society of Vacuum Coaters **49,** 314–318 (2006).

[9] J. Johnson, "Computationally modeling the effects of surface roughness on soft x-ray multilayer reflectors," Master's Thesis (Brigham Young University, Provo, UT, 2006).

[10] J. Jackson, Senior Thesis (Brigham Young University, Provo, UT, 2007).

[11] A. L'Hullier and P. Balcou, "High-order harmonic generation in rare gases with a 1-ps 1053-nm laser," Phys. Rev. Lett. **70,** 774–777 (1993).

[12] A. Rundquist, C. D. III, Z. Chang, C. Herne, S. Backus, M. M., and H. Kapteyn, "Phase-matched generation of coherent soft x-rays," Science **280,** 1412–1415 (1998).

[13] E. Takahashi, Y. Nabekawa, T. Otsuka, M. Obara, and K. Midorikawa, "Generation of highly coherent submicrojoule soft x-rays by high-order harmonics," Phys. Rev. A **66,** 1–4 (2002).

[14] D. Schulze, M. Dorr, G. Sommerer, J. Ludwig, P. Nickles, T. Schlegel, W. Sandner, M. Drescher, U. Kleineberg, and U. Heinzmann, "Polarization of the 61st Harmonic from 1053-nm Laser Irradiation in Neon," Phys. Rev. A **57,** 3003 (1998).

[15] E. Gullikson, S. Mrowka, and B. Kaufmann, "Recent developments in EUV reflectometry at the Advanced Light Source," Proc. of SPIE **4343,** 363–373 (2001).

[16] "ALS Quick Facts," http://www-als.lbl.gov/als/aboutals/alsquickfacts.html (Accessed May 21, 2007).

[17] S. L. Voronov, "Controlling laser high-order harmonic generation using weak counter-propagating light," Ph.D. dissertation (Brigham Young University, Provo, UT, 2003).

[18] J. Sutherland, "Phase-matching optimization of laser high-order harmonics generated in a gas cell," Master's Thesis (Brigham Young University, Provo, UT, 2005).

[19] J. Painter, "Direct observation of laser filamentation in high-order harmonic generation," Master's Thesis (Brigham Young University, Provo, UT, 2006).

[20] N. Brimhall, J. Painter, N. Powers, G. Giraud, M. Turner, M. Ware, and J. Peatross, "Measured laser beam evolution during high-order harmonic generation in a semi-infinite gas cell," Optics Express **15,** 1684–1689 (2007).

[21] J. Painter, M. Adams, N. Brimhall, E. Christiansen, G. Giraud, N. Powers, M. Turner, M. Ware, and J. Peatross, "Direct observation of laser filamentation in high-order harmonic generation," Optics Letters **31,** 3471–3473 (2006).

[22] E. T. J. Nibbering, G. Grillon, M. A. Franco, B. S. Prade, and A. Mysyrowicz, "Determination of the inertial contribution to the nonlinear refractive index of air, N2, and O2 by use of unfocused high-intensity femtosecond laser pulses," J. Opt. Soc. Am. B **14,** 650–660 (1997).

[23] S. Carusotto, E. Iacopini, E. Polacco, F. Scuri, G. Stefanini, and E. Zavattini, "Measurement of the Kerr constant of He, A, O2, N2, H2, and D2," Nuovo Cimento **5D,** 328–338 (1985).

[24] S. L. Chin, S. A. Hosseini, W. Liu, Q. Luo, F. Thberge, N. Akzbek, A. Becker, V. P. Kandidov, O. G. Kosareva, and H. Schroeder, "The propagation of powerful femtosecond laser pulses in optical media: physics, applications, and new challenges," Can. J. Phys. **83,** 863–905 (2005).

[25] S. Kazamias, F. Weihe, D. Douillet, C. Valentin, T. Planchon, S. Sebban, G. Grillon, F. Auge, D. Huilin, and P. Balcou, "High order harmonic generation optimization with an apertured laser beam," Eur. Phys. J. D **21,** 353 (2002).

[26] J. Sutherland, E. Christensen, N. Powers, S. Rhynard, J. Painter, and J. Peatross, "High harmonic generation in a semi-infinite gas cell," Optics Express **12,** 4430–4436 (2004).

[27] E. Christensen, "Direct Measurement of Absorption Rates for Laser High-Order Harmonics Generated in Helium and Neon," Senior Thesis (Brigham Young University, Provo, UT, 2005).

[28] Y. Tamaki, J. Itatani, Y. Nagata, M. Obara, and K. Midorikawa, "Highly efficient phase-matched high-order harmonic generation in self guided laser beam," Phys. Rev. Lett. **82,** 1422–1425 (1999).

[29] V. Tosa, E. Takahashi, Y. Nabekawa, and K. Midorikawa, "Generation of high-order harmonics in a self-guided beam," Phys. Rev. A **67,** 1–4 (2003).

[30] H. T. Kim, I. J. Kim, V. Tosa, Y. S. Lee, and C. H. Nam, "High brightness harmonic generation at 13 nm using self-guided and chirped femptosecond laser pulses," Appl. Phys. B **78,** 863–867 (2004).

[31] N. Terry, "Imaging High-Order Harmonics with a Curved Diffraction Grating," Senior Thesis (Brigham Young University, Provo, UT, 2000).

[32] D. Allred (private communication).

Index